Journal of Ocean Engineering and Marine Energy
https://doi.org/10.1007/s40722-021-00204-z

RESEARCH ARTICLE

Validation and comparison of turbulence models for predicting wakes of vertical axis wind turbines

Andrew Barnes[1] · **Daniel Marshall-Cross**[2] · **Ben Richard Hughes**[2,3]

Received: 18 December 2020 / Accepted: 12 June 2021

Abstract
Vertical axis wind turbine (VAWT) array design requires adequate modelling of the turbine wakes to model the flow throughout the array and, therefore, the power output of turbines in the array. This paper investigates how accurately different turbulence models using 2D computational fluid dynamics (CFD) simulations can estimate near and far wakes of VAWTs to determine an approach towards accurate modelling for array design. Three experiments from the literature are chosen as baselines for validation, with these experiments representing the near to far wake of the turbine. Five URANS turbulence models were chosen due to their common and potential usage for VAWT CFD: models k–ω SST, k–ω SST LRN, k–ω SSTI, transition SST, and k–k_l–ω. In addition, the lifting line-free vortex wake (LLFWV) model was tested as an alternative to CFD for the far turbine wake where it was appropriate for use. The results for turbulent kinetic energy and vorticity were compared for the first experiment, whilst streamwise and cross-stream velocity were used for the other two experiments. It was found that none of the turbulence models tested or LLFVW produced adequate estimations within the methodology tested, however, transition SST produced the closest estimations. Further adjustments to the methodology are required to improve accuracy due to their large impact on results including use of 3D CFD, adjustment of surface roughness, and inlet flow characteristics.

Keywords VAWT · CFD · Wind energy · Renewable energy · Modelling

Abbreviations

ε	Turbulence dissipation
2D	Two dimensional
3D	Three dimensional
CFD	Computational fluid dynamics
D	Diameters
HAWT	Horizontal axis wind turbine
R	Radius
RANS	Reynolds averaged Navier Stokes
SPIV	Stereoscopic particle image velocimetry
TSR	Tip speed ratio
TKE	Turbulent kinetic energy
VAWT	Vertical axis wind turbine

1 Introduction

Vertical axis wind turbines (VAWTs) are an alternative wind turbine design to the traditional horizontal axis wind turbine (HAWT) design. VAWTs have some potential advantages including omnidirectionality, lack of necessity of a pitching mechanism, and increased performance for arrays (Dabiri 2011). In the offshore context, they offer better stability for floating turbines due to their low centre of gravity because the generator can be placed at or below sea level. The potential for higher power density arrays (Dabiri 2011) allows for greater utilisation of regions which demonstrate geographical advantage such as higher wind speeds or more suitable topography which would reduce levelised cost of energy. However, there are also disadvantages such as lower power coefficient and a more complex basic design. These disadvantages may be hard to address as VAWTs present a difficult flow problem to model due to effects of dynamic stall and highly variable angle of attack of the blades, alongside the more three-dimensional nature of the flow and greater interactions between blades. Computational ability has increased and, therefore, accurately modelling this flow has

✉ Andrew Barnes
andrew.barnes@strath.ac.uk

[1] Department of Mechanical and Aerospace Engineering, University of Strathclyde, Glasgow, UK

[2] Free Running Buildings, Sheffield, UK

[3] Department of Engineering, University of Hull, Hull, UK

Published online: 23 July 2021

become more viable for researchers, allowing for investigation of these disadvantages.

1.1 Simulations

Modelling VAWTs can be split into two categories: 2D and 3D. The effects of dynamic stall, angle of attack, and interactions between blades can be modelled in 2D for the common H-bladed VAWT, which is effectively an extrusion of a 2D pattern of aerofoils around a central shaft (Abdalrahman et al. 2017). However, 3D effects are also important due to the high aerodynamic impact of the struts from the shaft to the blades (Hand and Cashman 2017), alongside tip effects which have a greater impact for turbines with a lower aspect ratio (Galetta 2018). 3D effects are also more prominent in other VAWT designs such as Helical or Φ which cannot simply be considered as an extrusion of a 2D object due to their variation of aerofoil position with height. For H-bladed VAWTs, 3D effects are necessary to consider for a more accurate prediction of the power coefficient of the turbine (Gosselin 2015).

Computational fluid dynamics (CFD) is commonly used to model VAWTs, because it offers an accurate general-purpose method of analysing fluid dynamics problems. A major factor in the accuracy of CFD simulation is the turbulence model used, so careful consideration is required to ensure the most suitable choice of turbulence model. Large or detached eddy simulation (LES/DES)-based turbulence models offer supreme accuracy but require higher resolution meshes and a 3D approach, therefore, needing much higher computational resources (Rezaeiha et al. 2019a).

Alternatively, Reynolds averaged Navier Stokes (RANS) models can be used, which allow for faster analysis, including in 2D. Within RANS there are several popular models for the analysis of VAWTs, the most common option being k–ω SST (MacPhee and Beyene 2016; Balduzzi et al. 2016; Zanforlin 2018; Su et al. 2020; Kothe et al. 2020), followed by k–ε (Howell et al. 2010; Castelli et al. 2011; Lee and Lim 2015; Pan et al. 2020; Mohamed et al. 2020) and transition SST (Rezaeiha et al. 2018, 2019b; Asr et al. 2016). Previous studies have also used other models including Spalart–Allmaras which has shown to be inadequate (Daróczy et al. 2015; Danao et al. 2012), k–k_l–ω (Daróczy et al. 2015; Arab et al. 2017), and corrections of k–ω SST (Danao et al. 2012) and transition SST (Almohammadi et al. 2013) such as the low Reynolds number and curvature corrected versions. There is also uncertainty regarding which RANS model provides the most accurate results, with some articles making opposing conclusions, particularly regarding k–ω SST and transition SST (Danao et al. 2014; McLaren et al. 2012; Daróczy et al. 2015; Rezaeiha et al. 2019b). A contrast also exists amongst the literature between which models better predict the power output of VAWTs and which better predict the wake characteristics, which is problematic given that accurate prediction of both is necessary for analysing arrays.

The 2D approach has some limitations which are demonstrated in Jiang et al. (2020), with the flow at the tips being significantly distorted, an effect which cannot be modelled in 2D and so requires a 3D approach. However, it can be seen that this has limited effect on velocity at the midplane for sufficiently high aspect ratio blades, so 2D results remain a valid estimation for wake velocity downstream at the midplane up to a certain point downstream providing the VAWT design does not use struts at or near the midplane as per Bachant and Wosnik (2016). Boudreau and Dumas (2017) find this point to be approximately 2 diameters downstream whilst Jiang et al.'s results and the results from Lam and Peng (2016) imply that this point occurs beyond 5 diameters downstream. The discrepancy is likely to be the result of differences in tip speed ratio which result in Boudreau and Dumas' setup having greater vortex shedding due to the higher effective angle of attack of the blades as a result of the lower tip speed ratio compared to Jiang et al.'s experiment. Alongside, these are two experiments by Tescione et al. (2014) and Rolin and Porté-Agel (2018), where Tescione et al.'s experiment does not show the impact of tip effects at the midplane within the sampled region downstream, whilst Rolin and Porté-Agel shows an impact at the earliest sampled distance downstream, 2 diameters. Both Tescione et al. and Rolin and Porté-Agel show increased wake enlargement at the midplane which may be due to 3D effects, however, given that many 3D CFD results in the literature Lam and Peng (2016) and Boudreau and Dumas (2017) do not demonstrate this wake enlargement it is inconclusive whether using 3D CFD is currently a solution. Equally, this phenomena is not seen in all VAWT experiments so the cause remains unclear (Posa et al. 2016; Lei et al. 2017). This study will not consider the cause of this discrepancy and leave this for future research.

An alternative method to CFD is nonlinear lifting line-free vortex wake (LLFVW) implemented in the QBlade suite, which allows a 3D approach but with significantly reduced computational resources compared to both 2D and 3D CFD (Marten et al. 2018). This method is significant, because it allows for wake modelling which other rapid simulation methods like Blade Element Modelling do not allow for unless combined with CFD, making them much more computationally intensive.

1.2 Experiments

Several experimental methods can be used for the flow analysis of VAWTs. Wake characteristics are analysed by carrying out particle image velocimetry (PIV) or stereoscopic particle image velocimetry (SPIV). With PIV, the fluid is seeded with particles which are assumed to follow the same

fluid dynamics as the fluid, the particles are then tracked through the flow using a camera. This allows for instantaneous tracking of fluid velocity along a two-dimensional plane, which for VAWTs is typically recorded at the mid-span of the blades. SPIV adds a second camera to track velocity in a third axis. Hot-wire anemometers can also be used which measure velocity in a single dimension and are typically used to measure the velocity across the horizontal axis of a wind tunnel. Laser and acoustic Doppler velocimetry or Cobra probes can also be used, however, these only measure velocity at a single point.

Buchner et al. (2015) investigated the blade wake at the point when the blade is furthest upwind at three different tip speed ratios (TSRs) using SPIV. Buchner et al. (2015) also compared their results against a 2D CFD model using k–ω SST, finding that the k–ω SST model is a poor predictor of wake characteristics including turbulent kinetic energy (TKE), dissipation rate, and vorticity, especially at TSR = 2.0. Tescione et al. (2014) used SPIV to measure the velocity field in the near-turbine wake up to 2 turbine diameters (D) downstream at TSR = 4.5. A partner study by Castelein et al. (2015) used the same experimental setup for the blade wake at several different rotational points at TSR = 2.0 and TSR = 4.5. Posa et al. (2016) studied near-turbine wake velocity using PIV up to 1D downstream at two TSRs (1.35 and 2.21). Posa et al. compared these results to a 2.5D CFD model using LES and found that the predicted wake velocity was higher than the experimental results but proposed that this was due to differences in the domains and poor aspect ratio elements in the mesh of the CFD model.

Peng et al. (2016) used hot-wire anemometers and a cobra probe to measure velocity downstream of the mid-span of the turbine. Peng et al. recorded results up to 10D, but at a lower resolution of only 1D. Lam and Peng (2017) conducted a study using two turbines in co-rotating and counter-rotating formations with the same methodology as Peng et al. (2016). Tescione et al. (2014) and Peng et al. (2016) also recorded results in the vertical direction, which enables validation of 3D CFD models. Ferreira (2009) also utilises hot-wire anemometry. Li (2016) used ultrasonic anemometers to measure wake angle in both wind tunnels and the field, measuring along two lines placed 1 and 2 turbine diameters behind the turbine, respectively.

1.3 Research gap

Studies on similar topics have been conducted previously such as Rezaeiha et al. (2019b) which investigated wake velocity prediction across seven turbulence models, including a comparison with Tescione et al. (2014). They found that transition SST offered the best results although the other SST-based models performed similarly overall. However, Rezaeiha only investigated the near-turbine wake and not the blade wake. Rezaeiha used a mesh of 402,999 cells but did not verify the mesh or meshing methodology for wake modelling downstream of the turbine, so it is unclear whether the results are a valid representation of the models' performance. The study does not consider the impact of tip speed ratio and, therefore, changes in effective Reynolds number on accuracy, or the evolution from blade wake to the wake downstream of the turbine.

Lam and Peng (2016) also conducted a CFD study using Tescione et al.'s results, considering 2D and 3D simulations using the transition SST turbulence model, alongside a 3D simulation using improved delayed detached eddy simulation (IDDES). Lam and Peng showed that IDDES offered no advantage compared to 3D transition SST, however, 3D transition SST offered better predictions of the near-wake compared to 2D. This study does not consider differences between turbulence models using 2D CFD and focuses on the differences between 2 and 3D CFD rather than the accuracy of the models. It also does not consider the evolution of the wake from the blade to the downstream wake.

Daróczy et al. (2015) compare the performance of URANS turbulence models for 2D CFD against baseline experiments, but only considers the TSR/C_p curve and not the blade or turbine wake.

Whilst there have been comprehensive comparisons of turbulence models for 2D CFD of VAWTs in the literature there has been limited consideration for the wake and in particular how the wake evolves in the different turbulence models to affect the downstream wake estimations. The accuracy of predicting the downstream wake is key for developing array designs due to their high sensitivity to location (Barnes and Hughes 2019; Sahebzadeh et al. 2020).

This paper will investigate the CFD modelling of 2D flow effects around vertical axis wind turbines. Five turbulence models and LLFVW will be validated against three experiments, each experiment representing different regions of the VAWT wake. The results will then be used to investigate the effect of turbulence model on accuracy of wake prediction. Through understanding how inaccuracies in predicting wake propagation at the blade level affect the wake further downstream of the turbine, it will be possible to develop models which more accurately predict array performance and to minimise the computational time required to make VAWT array optimisation a more viable endeavour.

2 Methodology

This study will use experimental results from the literature as baselines to compare the accuracy of several turbulence models for predicting the propagation of VAWT wakes from near-blade wake to near-turbine wake.

Three experiments by Buchner et al. (2015), Tescione et al. (2014) and Castelein et al. (2015) were used to validate results of representative CFD simulations. These three experiments have been chosen as they represent different regions and conditions of a VAWT. Buchner investigates the near-blade wake at several tip speed ratios, TSR = 1.0, 2.0, 3.0, which are representative of typical operating TSRs of a VAWT. Tescione investigates the near-turbine wake which is important when considering the VAWT's surroundings, for example when investigating VAWT farms. Near turbine wake can be defined as up to 3D away from the shaft, because this region is commonly used for closely spaced arrays (Brownstein et al. 2019; Barnes and Hughes 2019; Sahebzadeh et al. 2020). Castelein investigates the near and far-blade wake which is the transition between the near-blade and near-turbine regions. These regions are visualised in Fig. 1. The experiments use turbines with high blade aspect ratios, struts far away from the midplane, and high or increasing tip speed ratios, which allow for the 2D CFD methodology to extend its validity further downstream from the turbine due to minimising the impact of 3D effects in the studied regions. This is confirmed for the Tescione experiment with tip vortex effects not reaching the midplane within the sampled region.

Five turbulence models were validated against these experiments. The models k–ω SST, k–ω SST LRN, k–ω SSTI, transition SST, and k–k_l–ω as these are a combination of popular and increasingly popular choices in previous literature on VAWTs due to their accuracy and suitability to aerofoil flow problems combined with lower computational resource requirements. LLFVW was also used for the (Tescione et al. 2014) validation as it is suitable for the turbine wake but not blade wake.

The simulations were verified using mesh cell count and simulation length measured in number of turbine rotations. Other criteria including time step and pressure–velocity coupling has been chosen using the results and recommendations of previous literature.

2.1 Model setup

All simulations used the settings described in Table 1. Coupled was used as it allows for equal performance at larger time steps (Balduzzi et al. 2016) and faster convergence (Daróczy et al. 2015). Second-order discretisations were used due to the loss of accuracy from lower order formulations with some turbulence models (Almohammadi et al. 2013). Bounded second-order implicit was used for the transient formulation. The convergence criteria was set to 10^{-5} for all residuals and the number of iterations was set accordingly at 100 to ensure this was always met.

Table 1 Recommended settings for VAWT CFD

Pressure–velocity coupling	Coupled
Spatial discretisation	Second order (upwind)
Transient formulation	Bounded second-order implicit

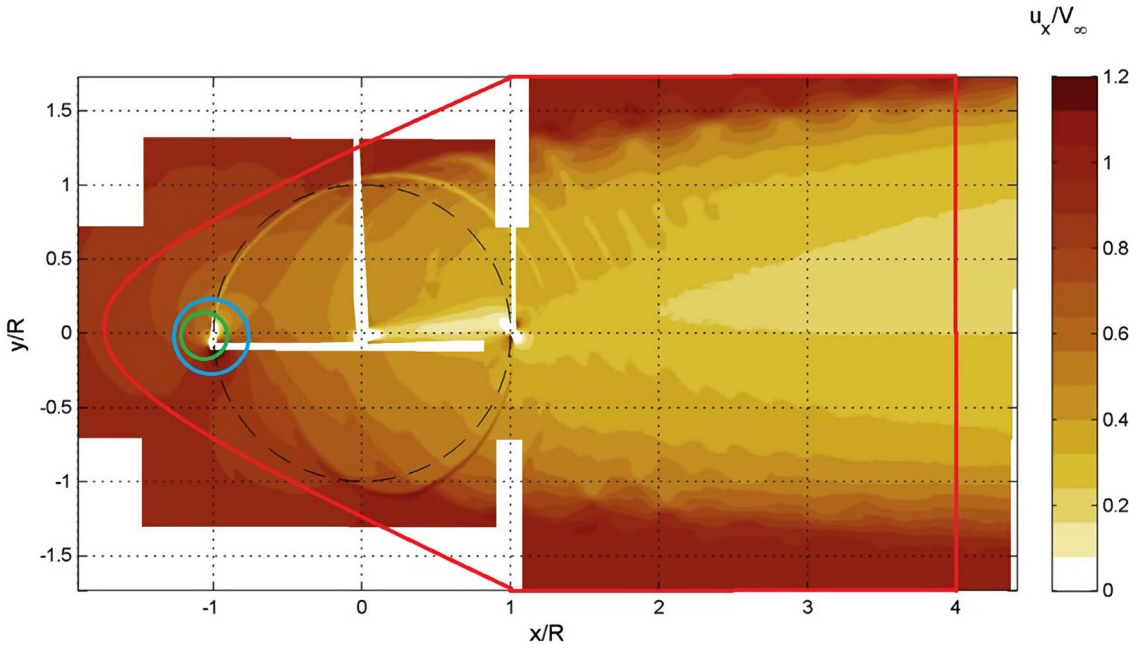

Fig. 1 Diagram of wake regions using streamwise velocity result modified from Tescione et al. (2014), where the green circle encloses the near-blade wake, blue the far-blade wake, and red the near-turbine wake (colour figure online)

Table 2 lists the domain configuration for the simulations, including the shape and dimensions of the domain and rotating region. For the simulation based upon Buchner's experiment, the domain shape and dimension were chosen to match those used in Buchner's CFD analysis. However, a ring was used for the rotating domain as this allows for a significant reduction in mesh cell count without affecting results as the PIV results were measured at the upwind-most position where the centre of the rotating domain will have an insignificant effect on results. For the Tescione and Castelein domain, the inlet and width dimensions were chosen to match Lam and Peng (2016) which conducted another 2D CFD validation of the Tescione experiment. An outlet length of 20*D* was used.

All CFD investigations was completed in ANSYS workbench versions 18.2 and 2019 R1, using DesignModeler for the geometry creation, ANSYS Meshing and FLUENT for meshing, FLUENT for the CFD simulations, and ANSYS Post-Processing to create any images of the CFD results.

The other setups were designed appropriately for the Buchner validations, and then again for the Tescione and Castelein validations. A single combined validation was sufficient for the latter two due to using the same experimental setup.

For QBlade, polars were determined for − 25° to 25° then extrapolated using the Viterna method. The LLFVW settings remained at default or the appropriate conditions to match the experiment, except for the panel method being set to sinusoidal with 20 panels, the tower being included with appropriate width and height, and turbulent wake convection being turned on.

2.2 Buchner validation setup

Buchner tests a variety of TSRs (1.0, 2.0, and 3.0) using the same rotational speed but varying the inlet velocity (15 m/s, 7.5 m/s, and 5 m/s). The models were compared on turbulent kinetic energy (TKE), turbulence dissipation, and vorticity.

A domain matching Buchner's CFD setup was used, with an outer domain diameter of ten diameters. The struts were not replicated due to the use of a 2D domain, which also prevents analysis of tip effects, however, the position of the PIV slice at mid-span minimises the effects of the struts and tip effects on the results. The shaft was also not included as the position of the blade at the chosen sampled rotational position by Buchner, on the far upwind side of the turbine, means the effect of the shaft is negligible. An inner rotating domain for the turbine with a diameter of 2D was used as while 1.25*D* was found to be sufficient (Rezaeiha et al. 2017), the referenced study used a turbine with a significantly lower solidity than the turbine used by Buchner, which will impact the size of the blade wake. The larger high-density mesh area will account for this to ensure greater accuracy of the blade wake. 50 inflation layers with a growth rate of 1.09 were applied to the blades with a first layer height of 1.955×10^{-5} m to provide $y^+ = 1$ which is necessary for good performance with SST models. The singularity at the trailing edge of the aerofoil was treating by trimming the trailing edge.

These settings were used to produce meshes with cell counts of 47,679 (low), 220,081 (medium), and 782,263 (high) seen in Fig. 2, with the high cell count mesh created from the medium mesh using the refinement tool in FLUENT. A rotational step of 0.5° was used as recommended by Rezaeiha et al. (2017). Simulation lengths of 1.5, 5, and 10 rotations were tested to determine the point of convergence.

Skin friction coefficient along one side of the blade length measured as fraction of chord was used to verify convergence of the mesh cell count and time step as this is a measure of the effects of flow against the blades and so can be used as a quantitative measure of the convergence of the wake. This is plotted in Fig. 3 where ten rotations using the medium density mesh and five rotations using the high-density mesh produce the same curve, so the medium mesh is chosen.

The different turbulence models and the experiment will be quantitatively compared upon the area of the wake, measured using a colour threshold in the software ImageJ, with the areas normalised against the area of the blade in the image.

2.3 Tescione and Castelein validation

Tescione tests a single condition with a fixed freestream velocity of 9.3 m/s and a TSR of 4.5, this was repeated in these simulations. The result of the experiment was the streamwise and cross-stream velocity values. While Castelein uses a slightly lower freestream velocity of 9.1 m/s,

Table 2 Domain shape for CFD simulations

	Buchner	Tescione and Castelein
Domain shape	Circle with 10*D* radius	Rectangle with semi-circular inlet of 5*D* radius and outlet length of 20*D*
Rotating region shape	Ring with 2D outer and 0.75*D* inner diameter	Circle with 1.25*D* diameter
Blockage ratio	5%	10%

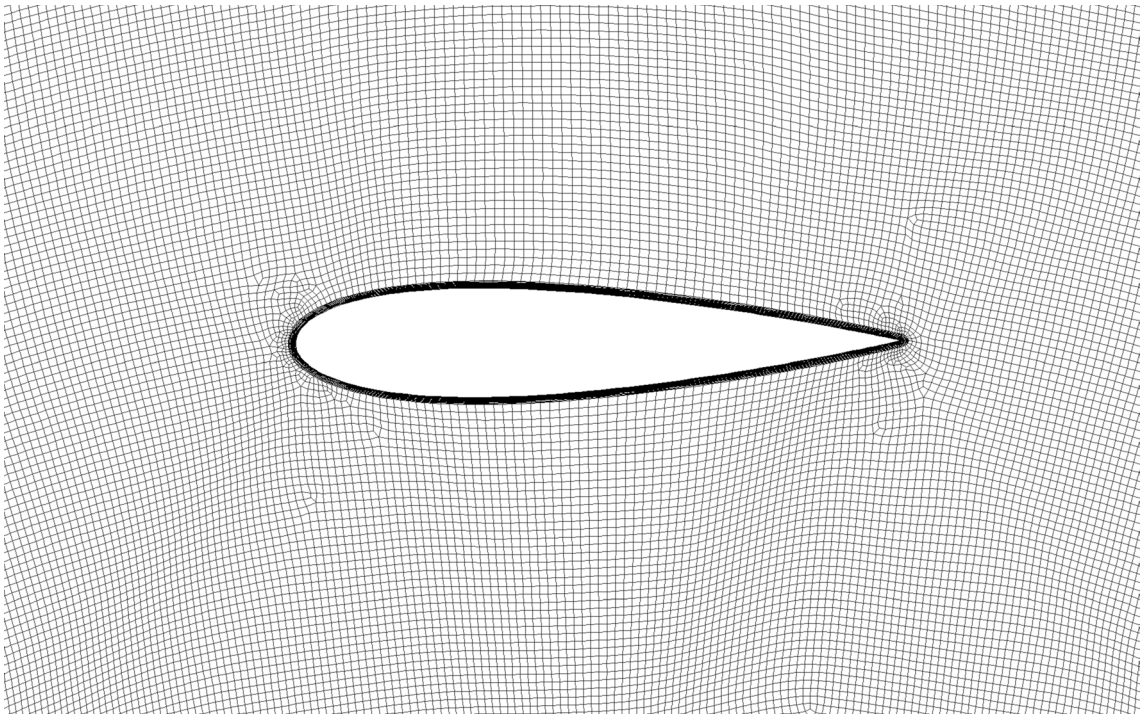

Fig. 2 High cell count mesh used for Buchner validation

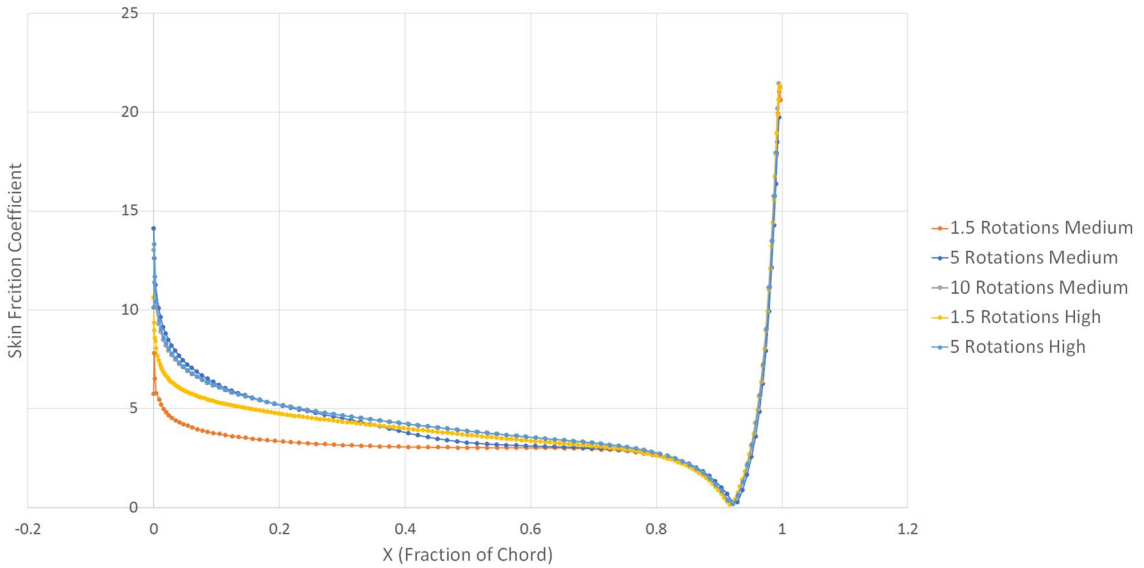

Fig. 3 Comparison of skin friction coefficient using different mesh cell counts and lengths of simulation, using k–ω SST turbulence model at TSR = 1.0. Markers represent sampled points

however, the small change this causes to Reynold's number means the effect on results is insignificant.

Tescione used a wind tunnel test section with measurements of $13.7D \times 6.6D \times 8.2D$ and this was replicated in the 2D models using a $13.7D \times 6.6D$ test section. As Tescione does not state the location of the turbine with this domain, it was placed $5D$ downstream from the velocity inlet, the same as used by Lam and Peng (2016) for another validation of Tescione. The shaft was replicated in the 2D model as it effects downwind wake velocity, as shown by the images produced by Tescione et al. (2014). The struts were not replicated due to the position of the

stereoscopic particle image velocimetry (SPIV) slice at mid-span minimising their effects on the results and because it is not possible in 2D simulations.

A high cell count mesh of 1,351,811 cells was produced with a dense section following the turbine to accurately capture the near-turbine wake, which was not necessary for the Buchner validation as the area of interest was limited to the near-blade wake and so did not extend downwind of the turbine region. The high cell count combined with using the same meshing technique as for the Buchner simulation ensures converged results. Y^+ value was set to 1. A time step of 1×10^{-4} s was used, equivalent to 0.5°, which is sufficient for the high TSR scenario used here (Rezaeiha et al. 2017; Danao et al. 2014). The simulations were run for 15 revolutions or until there was no change at 3 diameters downstream of the turbine centre after 1 revolution, whichever required the highest number of revolutions. This is much higher than Buchner due to the necessity of further wake propagation to produce converged results in the downstream wake. For the time-averaged results, a single sample was taken every time step for one revolution using the Data Sampling for Time Statistics feature in FLUENT.

For comparing simulation results against Tescione, the maximum percentage and absolute deviation from the experimental results will be recorded, whilst for comparisons against Castelein, the area of comparable colour bands will be recorded.

3 Results

3.1 Near blade wake

Buchner produced results for turbulent kinetic energy (TKE), dissipation rate ε, and vorticity at TSRs 1.0, 2.0, and 3.0. Out of these both TKE and vorticity have been replicated with CFD simulations using the different models.

First, the quantitative results can be considered using the size of the wake, shown in Tables 3 and 4.

Large deviations can be seen between nearly all simulations and the experiment, with significant variation between the different measures of wake size also. The largest deviations occur for positive vorticity at TSR = 2.0 with overestimations greater than 140% for most models, with the exception of transition SST which demonstrates its

Table 3 Comparing the normalised area of the wake of different turbulence models against the experiment

Condition	TKE Normalised Area	Deviation from Experiment (%)	Positive Vorticity Normalised Area	Deviation from Experiment (%)	Negative Vorticity Normalised Area	Deviation from Experiment (%)
Tip Speed Ratio=1						
k-ω SST	8.100996	-48.0104	3.957165	-17.0163	5.59904	-57.2135
k-ω SST LRN	8.282709	-46.8442	3.846102	-19.3454	5.715527	-56.3233
Transition SST	7.2014	-53.7837	3.292273	-30.9594	6.282315	-51.9921
k-k_l-ω	15.64672	0.415647	2.672725	-43.9517	6.99874	-46.5173
Experiment	15.58195		4.768608		13.086	
Tip Speed Ratio=2						
k-ω SST	1.472804	-43.2037	1.899158	153.4491	1.217395	-44.0796
k-ω SST LRN	2.044511	-21.1568	1.850582	146.9665	1.355737	-37.725
Transition SST	1.871781	-27.8179	1.050964	40.25468	1.258005	-42.2142
k-k_l-ω	3.221853	24.24548	1.810662	141.639	1.331055	-38.8587
Experiment	2.593135		0.749325		2.177015	
Tip Speed Ratio=3						
k-ω SST	1.035341	-57.9868	1.054984	30.70108	0.82911	-50.5774
k-ω SST LRN	0.608199	-75.3199	1.088277	34.8257	0.857889	-48.8619
Transition SST	1.187454	-51.8143	0.976523	20.98061	0.848358	-49.43
k-k_l-ω	3.706248	50.39594	0.727172	-9.91126	0.825725	-50.7792
Experiment	2.464327		0.807173		1.677594	

Table 4 Average of the absolute deviation from experimental results for each turbulence model

Turbulence model	Average absolute deviation (%)
k–ω SST	55.80423
k–ω SST LRN	54.15208
Transition SST	41.02743
k–k_l–ω	45.19047

improved performance in the laminar-to-turbulent transition region. The normalised wake area for the turbulence models for negative vorticity is relatively consistent, with the percentage difference between the models decreasing as TSR increases. Compared to the other turbulence models and the experiment, k–k_l–ω tends to overestimate the turbulent kinetic energy wake area whilst producing lower estimates of positive vorticity.

In terms of the average absolute deviation shown in Table 4, transition SST offers the lowest absolute deviation, followed by k–k_l–ω. Both of these models have lower average deviation due to improved performance in a number of circumstances compared to other models rather than consistently improved accuracy.

The results can then be considered qualitatively to understand some of the causes of these deviations.

The upper left image in Fig. 4 shows Buchner's PIV results for turbulent kinetic energy at TSR = 1.0, showing a wake with a height of 0.11 m, a circulation at the leading edge which is approximately at a right angle to the chord, one vortex at the trailing edge and one vortex above the three-quarter chord position, and a tail which extends from between the two vortices.

The other images in Fig. 4 show the CFD results for the four turbulence models at TSR = 1.0. Transition SST produces the closest representation of the wake with vortices at the trailing edge and above the three-quarter chord position. A faint tail is also found alongside the leading edge circulation. However, it fails to predict the angle between the leading edge circulation and chord, and underestimates the size of the wake and TKE. The other models fail to predict the position of the vortices but predict a stronger tail. The k–k_l–ω model also produces a better prediction of the leading edge circulation.

For vorticity at TSR = 1.0 in Fig. 5, two vortices are seen with a leading edge circulation and trailing edge circulation. The upper vortex has negative vorticity, while the trailing edge vortex has positive vorticity. A small triangle of positive vorticity is also seen behind the leading edge circulation.

As shown in the other images in Fig. 5, vorticity is overestimated significantly. The k–ω SST models produce the most similar shape of the wake overall. k–k_l–ω produces a more accurate prediction at the leading edge with a thinner leading edge circulation and a smaller triangle of positive

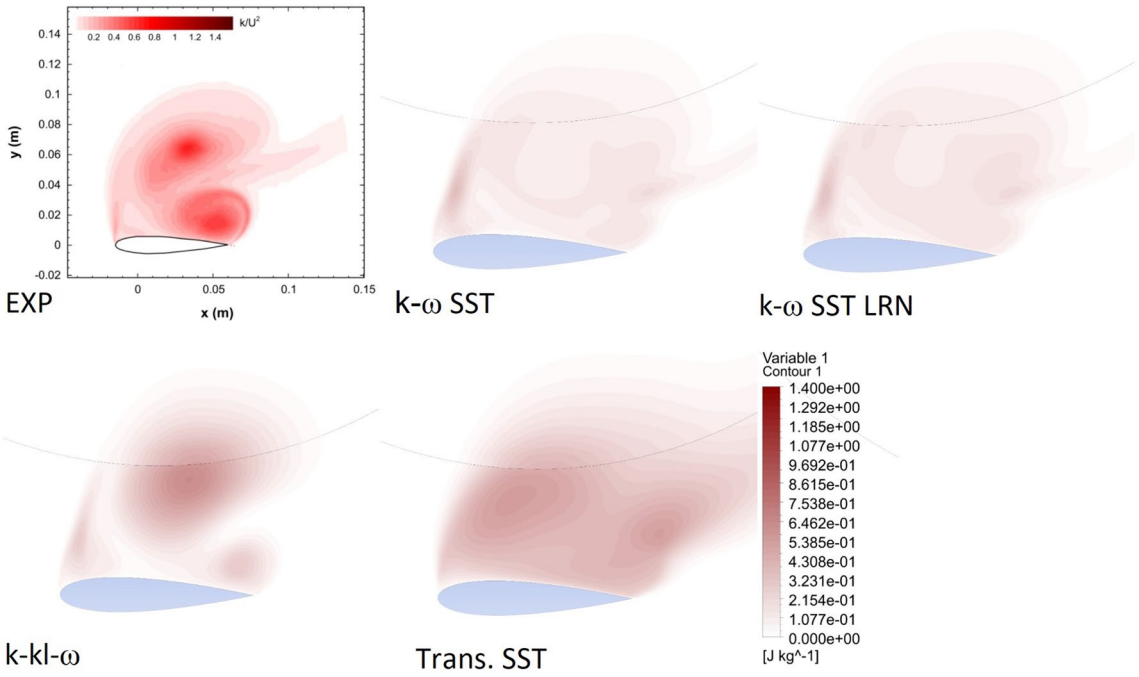

Fig. 4 Upper left: Buchner's experimental result for turbulent kinetic energy at TSR = 1.0 (Buchner et al. 2015), upper centre: k–ω SST, upper right: k–ω SST LRN, lower left: transition SST, lower middle: k–k_l–ω

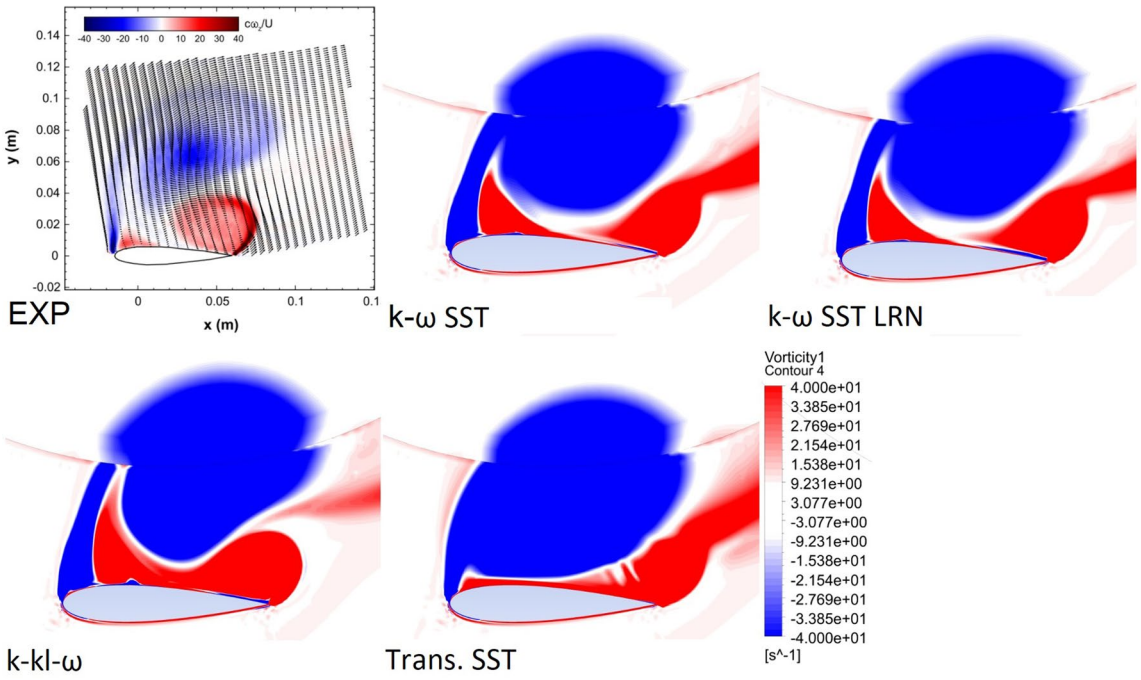

Fig. 5 Upper left: Buchner's experimental result for vorticity at TSR = 1.0 (Buchner et al. 2015), upper centre: k–ω SST, upper right: k–ω SST LRN, lower left: transition SST, lower middle: k–k_l–ω

vorticity, but underestimates the size and impact of the trailing edge vortex as shown in the quantitative results.

Figure 6 shows the TKE experimental result at TSR = 2.0, with a separation of very high TKE stemming from the leading edge, followed by reattachment, then a tail originating at the trailing edge.

Transition SST is the best predictor of the leading edge separation amongst the models shown in Fig. 6 but significantly underestimates the size of the separation and does not predict the reattachment. The size of the tail is also underestimated significantly.

The experimental vorticity result in the top left of Fig. 7 shows the same pattern as the turbulent kinetic energy result, with a negative vorticity leading edge separation followed by reattachment. At the trailing edge, the tail is split into an upper negative vorticity region and a lower positive vorticity region.

Vorticity is again significantly overestimated in the CFD shown in the other images in Fig. 7 compared to the experimental results and the overall prediction is poor. All models predict the negative vorticity upper tail and positive vorticity lower tail, although k–ω SST LRN and k–k_l–ω predict shorter but wider tails.

The experimental result for turbulent kinetic energy at TSR = 3.0 shown in the top left of Fig. 8 has a nearly flat wake from a separation close to the leading edge, with another trailing edge separation that produces a tail. In the vorticity map in Fig. 9, there is a positive vorticity lower tail and negative vorticity upper tail from the trailing edge.

All the models in Figs. 8 and 9 fail to predict the position of the initial separation, with all but k–ω SST estimating occurrence of separation at one-third chord. From the vorticity maps, it is seen that this is due to a positive vorticity region covering the leading edge, which pushes separation backwards. These differences may be due to surface roughness on the experimental blades which can affect separation (Iverson et al. 2019).

Overall, transition SST offers the most robust performance out of the tested turbulence models, however, accuracy is still poor for the blade wake so other modelling techniques may be required for near-blade wake analysis.

3.2 Near turbine wake

The Tescione experiment provides results of the wake surrounding and closely following the turbine, investigating time-averaged streamwise and cross-stream velocity.

First, the deviation between the simulation and experimental results can be considered in Table 5 for streamwise velocity, where transition SST demonstrates the smallest deviation from the experimental baseline at all distances downstream. However, the difference in accuracy between the turbulence models is limited with predictions from both k–ω SST and k–k_l–ω remaining within 1% of Inlet Velocity.

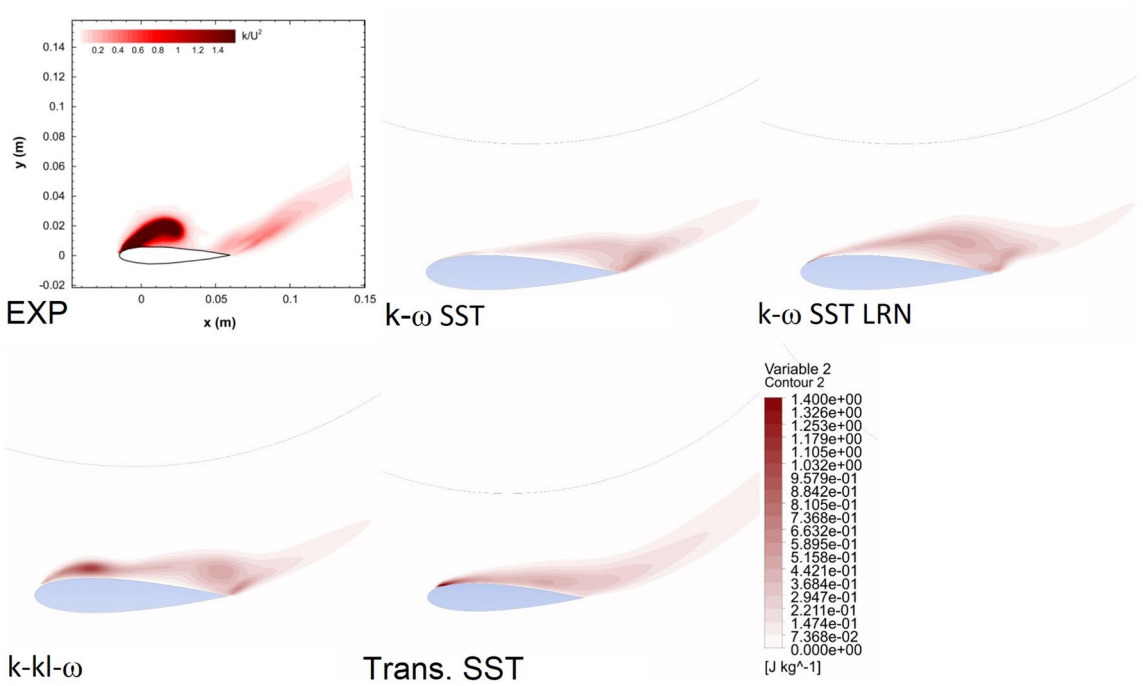

Fig. 6 Upper left: Buchner's experimental result for turbulent kinetic energy at TSR = 2.0 (Buchner et al. 2015), upper centre: *k–ω* SST, upper right: *k–ω* SST LRN, lower left: transition SST, lower middle: *k–k*$_l$*–ω*

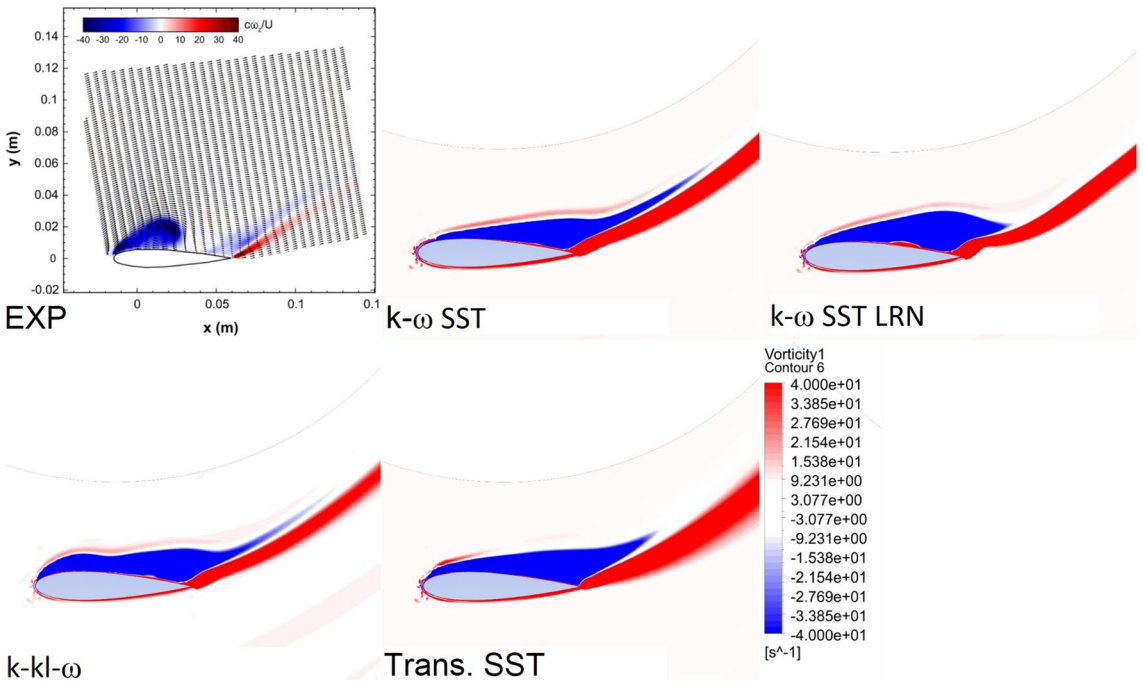

Fig. 7 Upper left: Buchner's experimental result for vorticity at TSR = 2.0 (Buchner et al. 2015), upper centre: *k–ω* SST, upper right: *k–ω* SST LRN, lower left: transition SST, lower middle: *k–k*$_l$*–ω*

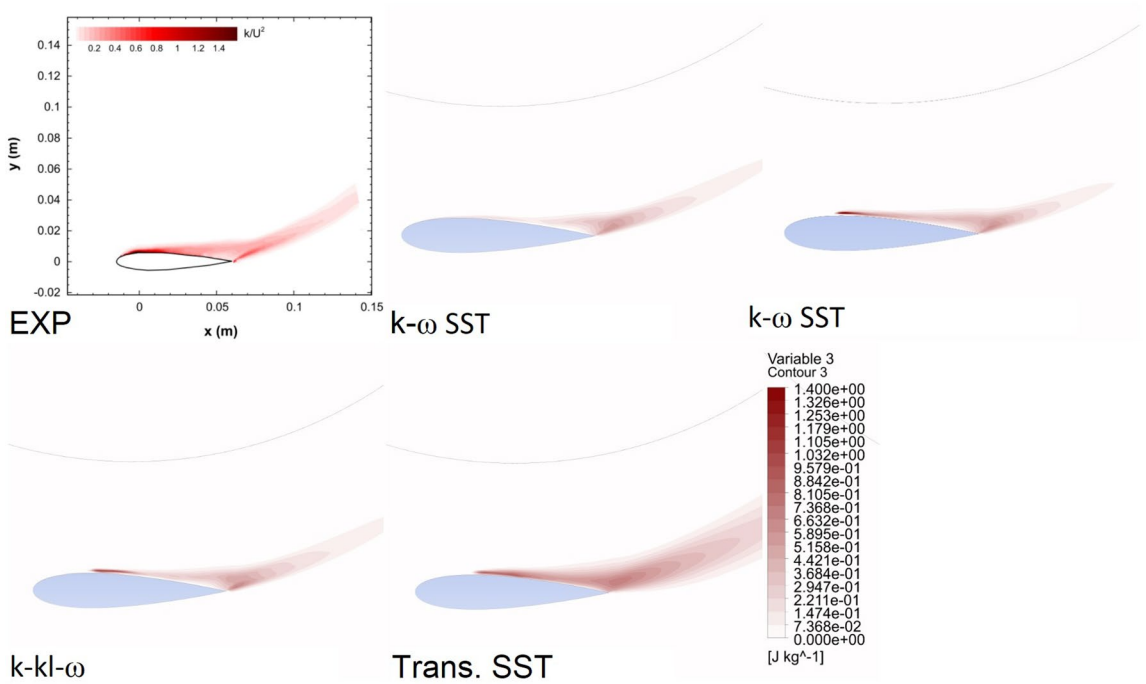

Fig. 8 Upper left: Buchner's experimental result for turbulent kinetic energy at TSR = 3.0 (Buchner et al. 2015), upper centre: k–ω SST, upper right: k–ω SST LRN, lower left: transition SST, lower middle: k–k_l–ω

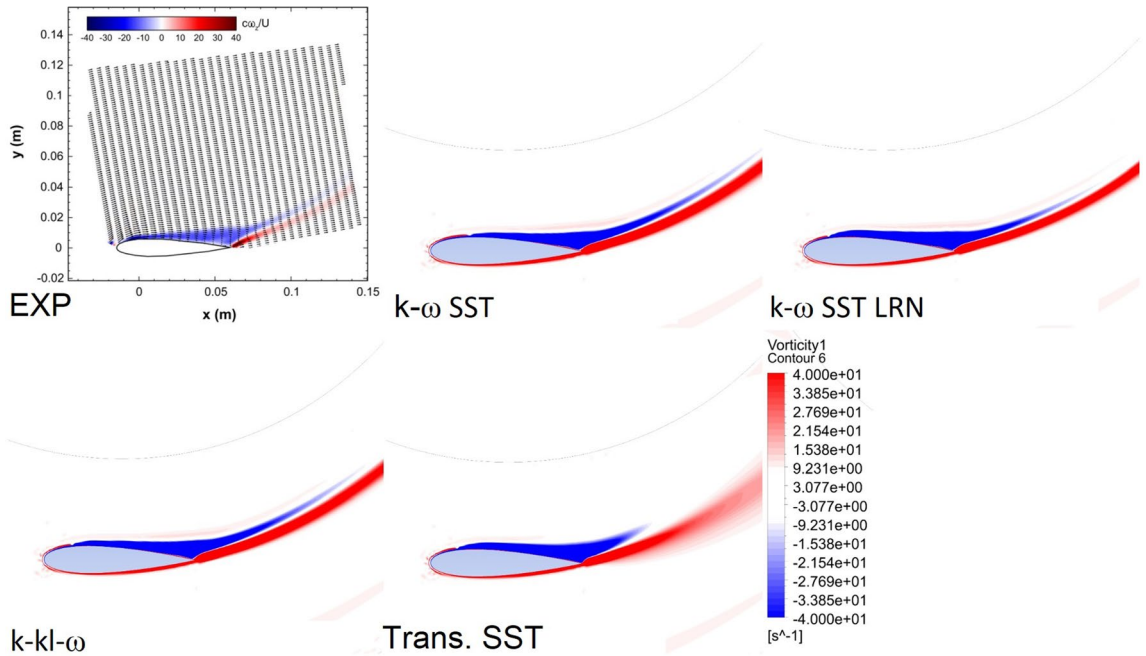

Fig. 9 Upper left: Buchner's experimental result for vorticity at TSR = 3.0 (Buchner et al. 2015), upper centre: k–ω SST, upper right: k–ω SST LRN, lower left: transition SST, lower middle: k–k_l–ω

QBlade shows poor results with significantly larger deviations from the experiment. All models demonstrate increasing error from the experiment further downstream.

In Table 6, the cross-stream velocity is considered, showing that k–k_l–ω offers the lowest error from the experiment up to 2.5R downstream. Then, transition SST offers the best

Table 5 Deviation between simulation predictions of streamwise velocity downstream of the VAWT compared to the (Tescione et al. 2014) experiment

Distance downstream (R)		Transition SST	k–k_l–ω	k–ω SST	k–ω SST LRN	QBlade
1.5	Average absolute deviation (m/s)	0.564303	0.635303	0.638241	0.618519	3.803342
	As % of inlet velocity	6.067772	6.831212	6.862807	6.650737	40.89615
2.5	Average absolute deviation (m/s)	0.700645	0.757043	0.784734	0.832268	4.442899
	As % of inlet velocity	7.533823	8.140249	8.437998	8.949115	47.7731
4	Average absolute deviation (m/s)	0.98027	1.018481	1.071425	0.447744	5.950974
	As % of inlet velocity	10.54053	10.9514	11.5207	13.4621	63.98897

Table 6 Deviation between simulation predictions of cross-stream velocity downstream of the VAWT compared to the (Tescione et al. 2014) experiment

Distance downstream (R)		Transition SST	k–k_l–ω	k–ω SST	k–ω SST LRN
1.5	Average absolute deviation (m/s)	0.434392	0.344364	0.455149	0.656757
	As % of U0	4.670881	3.70284	4.894072	7.061903
2.5	Average absolute deviation (m/s)	0.403252	0.24388	0.479449	0.471089
	As % of U0	4.336048	2.622365	5.155366	5.065473
4	Average absolute deviation (m/s)	0.191841	0.227459	0.31445	0.21692
	As % of U0	2.062801	2.445797	3.381181	2.332476

Table 7 Combined deviation between simulation predictions for both streamwise and cross-stream velocity downstream of the VAWT compared to the (Tescione et al. 2014) experiment

Distance downstream (R)		Transition SST	k–k_l–ω	k–ω SST	k–ω SST LRN
1.5	Average absolute deviation	0.998695	0.979667	1.09339	1.275276
	As % of U0	10.73865	10.53405	11.75688	13.71264
2.5	Average absolute deviation	1.103898	1.000923	1.264183	1.303357
	As % of U0	11.86987	10.76261	13.59336	14.01459
4	Average absolute deviation	1.17211	1.24594	1.385875	0.664665
	As % of U0	12.60334	13.3972	14.90188	15.794576

accuracy at 4R downstream, with k–ω SST LRN and k–k_l–ω offering slightly reduced accuracy.

Combining the streamwise and cross-stream velocity errors in Table 7, both transition SST and k–k_l–ω offer good accuracy with k–k_l–ω offering improved accuracy up to 2.5R downstream. This may indicate that transition SST is more appropriate for arrays where the turbines are placed greater than 2.5R apart, whilst k–k_l–ω is appropriate for distances up to 2.5R. k–ω SST may be useful to initialise simulations due to being less computationally intensive, followed by switching to transition SST or k–k_l–ω.

To understand the cause of the deviations, the graphs and contour maps of streamwise velocity can be considered, with markers representing sampled points.

From the experimental results in Fig. 10, it is shown that the wake in the experiment has reducing velocity further away from the turbine and there is a greater velocity deficit to the upwind stroke side of the turbine (positive X values), which increases further away from the turbine. The minimum velocity point moves from 2.5 m/s at approximately $x = +0.05$ m for 1.5R downstream to 1.8 m/s at $x = +0.25R$ for 4.0R downstream.

The turbulence models show good estimations of the downwind stroke time-averaged streamwise velocity (negative X values) but fail to predict the greater deficit on the upwind stroke as seen in Fig. 11. This inaccuracy becomes greater further downwind. This has been seen in other research for 2D and 2.5D VAWT simulation by Bachant and Wosnik (2016) and Rezaeiha et al. (2017), though appears to be solved using a 3D approach (Lam and Peng 2016). It should be noted that Rezaeiha's paper uses Tescione's experiment as their experimental reference, and Bachant's turbine is at the same scale with similar magnitude of blade Reynolds number. Further research needs to be conducted at commercial scale Reynolds numbers of 10^7 to determine whether this is a factor in accuracy of prediction of the turbine wake for utility scale turbines.

k–ω SST and transition SST produced the most accurate results, with transition SST better predicting the wider low-velocity region on the upwind side from $x = 0.2$ m to 0.5 m for 1.5R and 2.5R, and $x = 0.1$ m to 0.5 m for 4.0R. k–k_l–ω showed a droop on the downwind stroke side compared to the experiment and other turbulence models. It also showed a smoother wake profile throughout the rotations which could affect results for farm design as the intra-rotation

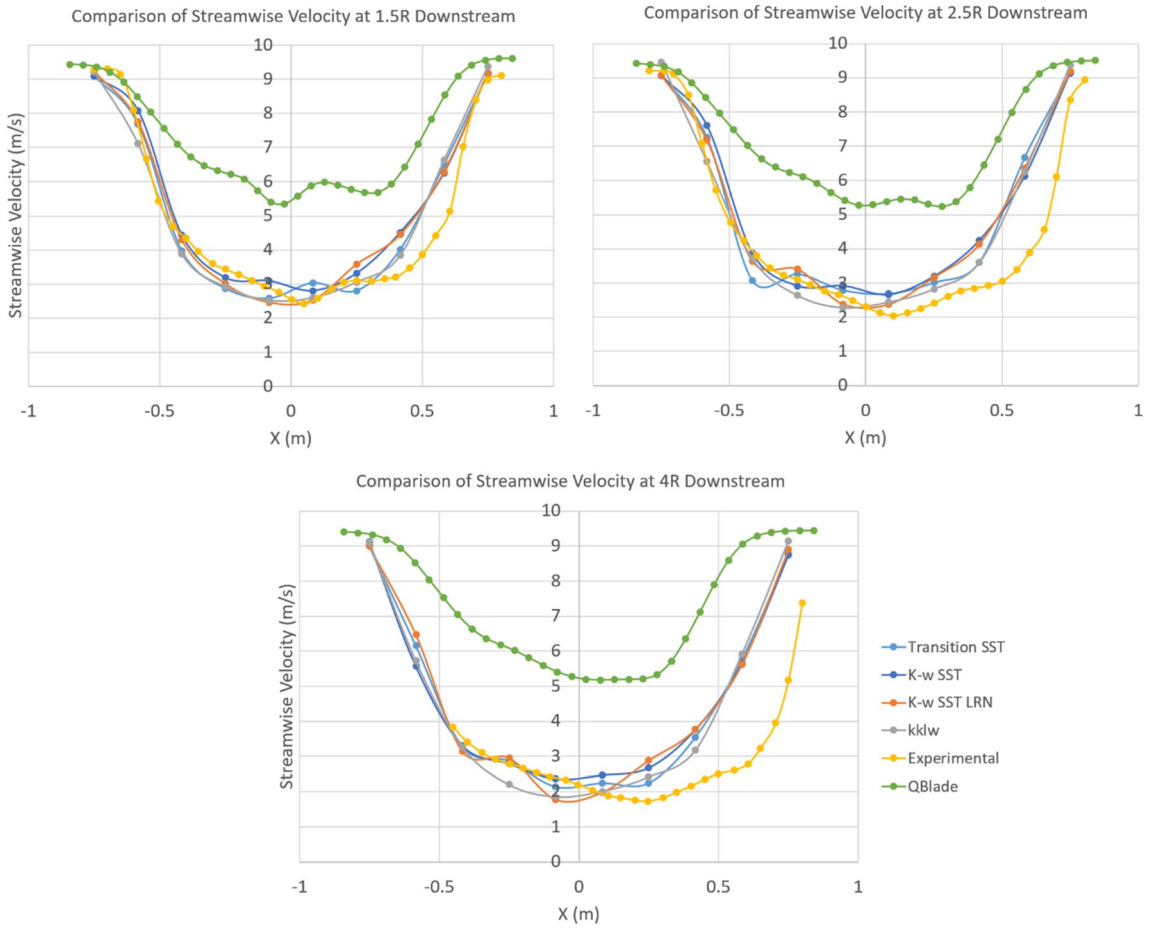

Fig. 10 Comparing turbulence model results with experimental results for streamwise velocity at 1.5*R* (upper left), 2.5*R* (upper right), and 4.0*R* (lower) downstream

fluctuations may alter power output of downwind turbines in some circumstances. Using cubed root of the mean of the cubed velocity fields would help designers account for this as this measures the average power at a given point (Wahl 2007). This relationship also means there would be relatively little difference in terms of power prediction for downstream turbines between k–ω SST and transition SST, because the regions where their predictions differ have low velocities.

Considering cross-stream velocity in Fig. 11, better accuracy is seen at smaller distances downwind, with k–ω SST LRN producing the most similar results to the experiment at 1.5*R* downwind, although the gradient of the velocity change is lower than expected from the experimental results. At 2.5*R* downwind, all models except for k–k_l–ω show very oscillatory behaviour so there is no clear better turbulence model for predicting cross-stream velocity at this distance downstream. At 4.0*R,* the oscillatory behaviour becomes an even greater issue. For downwind turbines in the mid-wake, especially on the upwind stroke side, the cross-stream velocity constitutes a significant component of the total velocity vector, so accounting for this in turbine placement and variable pitch algorithms will be necessary to ensure optimal operation.

The results can also be compared against previous CFD in the literature for the Tescione et al. (2014) experiment such as Rezaeiha et al. (2019b) and Lam and Peng (2016) shown in Fig. 12. Lam and Peng's results using the k–ω SST model demonstrate an overestimation at all points whilst Rezaeiha, Montazeri, and Blocken shows good agreement or small overestimation in the negative X region, whilst k–ω SST and transition SST in the current study underestimate between − 0.4 and − 0.1 m, with transition SST showing a greater deviation. In the positive X region, the current study demonstrates a significantly reduced deviation from the experiment using k–ω SST and transition SST compared to Lam and Peng, and Rezaeiha, Montazeri, and Blocken's use of the same models. The oscillation at the centre in Rezaeiha, Montazeri, and Blocken's results is also not seen in either the current study or Lam and Peng. This may be due to the choice of pressure–velocity coupler or the different meshes used, because these studies use similar methodologies otherwise.

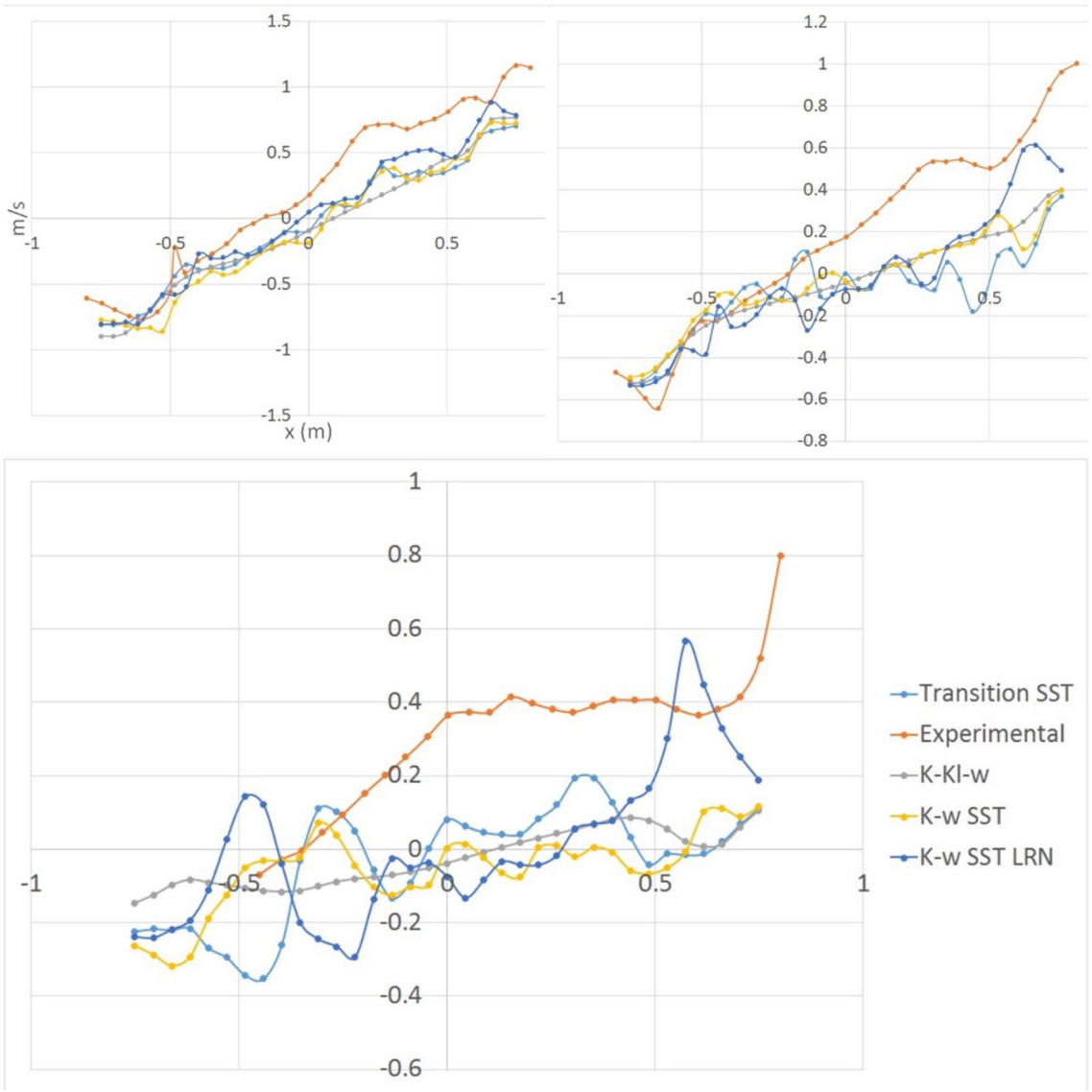

Fig. 11 Comparing turbulence model results with experimental results for cross-stream velocity at 1.5*R* (upper left), 2.5*R* (upper right), and 4.0*R* (lower) downstream

3.2.1 Streamwise velocity wake visualisation

By inspecting the full plane of the wake, it is possible to visualise characteristics of the flow to help further understand the velocity graphs. Instantaneous values were used here for the CFD results.

It can be determined by inspection of Fig. 13 that the k–k_l–ω model provides the most similar prediction of the instantaneous inner wake streamwise velocity with the other models failing to predict the more cohesive wake formation seen in Tescione's results. All the models overestimate the velocity at the edges of the wake, and k–k_l–ω predicts a much smoother wake pattern than the experiment and other models. This is an issue for array design if the outer wake is an important variable in the performance of downwind turbines, and in a 3D scenario, there will be additional effects from wake contraction in the Z axis alongside tip vortex effects which are not present in the 2D simulation.

All models underestimate the velocity deficit caused by the shaft, with transition SST producing slightly higher velocity predictions than the other models. The SST models including k–ω SST, k–ω SST LRN, and transition SST are better predictors of the blade wake velocity with the impact still being accurately predicted until the third wake artefact downstream. The LRN model produces wavy sprites at the wake edge, however, while the experimental results show smoother sprites, so the standard k–ω SST and transition SST are better in this regard.

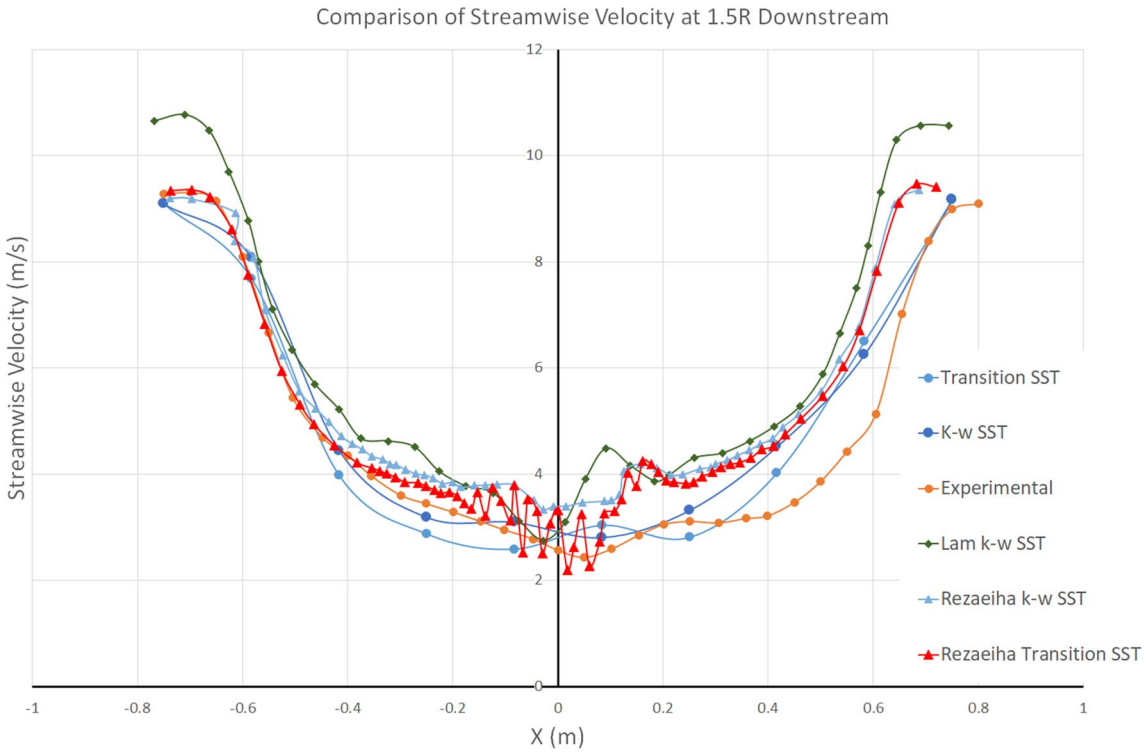

Fig. 12 Comparison of k–ω SST and transition SST streamwise velocity results at 1.5R downstream for the current study and previous literature Rezaeiha et al. (2019b) and Lam and Peng (2016)

As shown in the velocity graphs also, the wake tends towards the centre or downwind side in the CFD models, whereas it tends further towards the upwind side on the experiment.

Differences occur in the visualised wakes due to inaccurate replication of the contour boundaries, as while the contour colour scheme has been replicated it is not a perfect copy. In the future, it would be preferable to use a scheme with smaller velocity bands and a larger colour gradient to improve comparability.

3.2.2 Cross-stream velocity wake visualisation

From Fig. 14, a significant departure from the experimental results is seen in all turbulence models. All models show smaller regions with cross-stream velocity near zero, alongside larger areas of negative velocity on the upwind side and positive velocity on the downwind side.

3.2.3 Discussion of Tescione validation

All the CFD models show good prediction of wake velocity on the upstream side of the turbine region, however, transition SST has a more accurate prediction on the downstream side. Wake artefacts from previous revolutions of the blade with the turbine region are positioned further downstream than their equivalents in the experimental results, and they have a smaller radius of curvature compared to the experiment also. This makes any comparison difficult as any interaction between past blade wakes and the rotating blades could alter results significantly.

There is also a repetition of k–k_l–ω producing very different results compared to the other turbulence models, showing a lower cross-stream velocity on the edges of the wake compared to the experiment, in contrast to the high streamwise velocity in these areas.

The difference in these results compared to Rezaeiha et al. (2017) could be due to two variables: meshing or pressure–velocity coupler. The mesh used here has a much higher number of cells compared to Rezaeiha's (1,351,811 vs. 402,999) and in particular, this mesh uses a refined wake zone which was not used by Rezaeiha who only refined around the blade regions. The other change is that Rezaeiha used the SIMPLE pressure–velocity coupler whereas coupled was used here. A verification was conducted to determine whether this was the cause of the difference in results, however, the difference was negligible as shown in Fig. 15.

Overall, transition SST offers the most accurate model, however, users should be aware of velocity being overestimated in the upwind side wake. k–ω SST offers a good alternative for conducting a large number of simulations due to

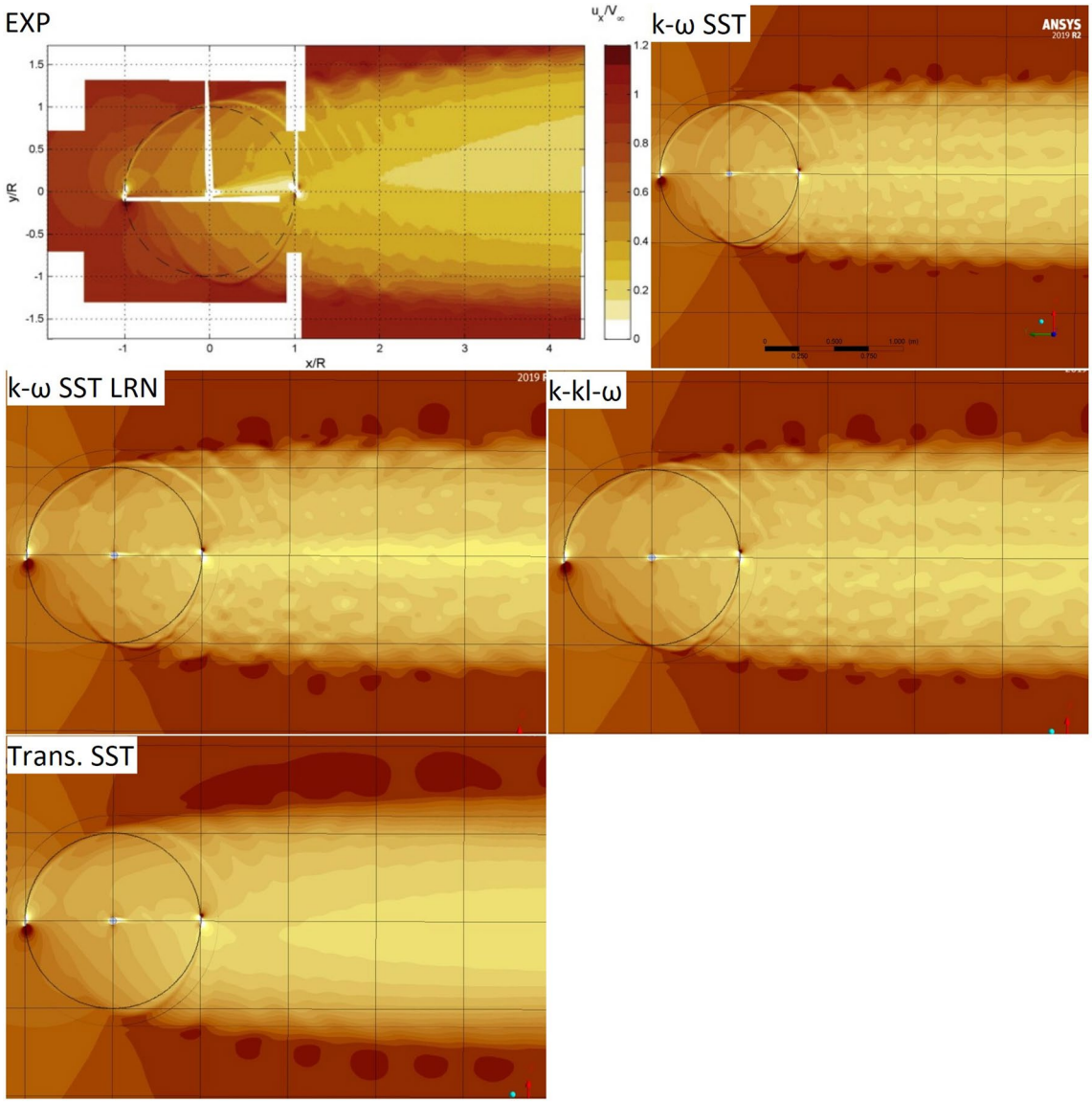

Fig. 13 Comparison of experimental SPIV results for streamwise velocity by Tescione and CFD results by turbulence model. Upper left: Tescione's results (Tescione et al. 2014), upper right: *k–ω* SST centre left: *k–ω* SST LRN, centre right: transition SST, Lower: k–k_l–ω

its lower computational time and similar accuracy. It is also clear that small deviations in methodology can make a significant difference for VAWT wake prediction as shown by the disparities in results between the current study, Rezaeiha et al. (2019b) and Lam and Peng (2016).

3.3 Far blade wake

Castelein examines the blade wake at different azimuthal positions at two TSRs, however, here only one TSR (4.5) will be investigated.

Table 8 considers the size of comparable regions of the blade wakes, divided into high-velocity regions above 6.5 m/s and low-velocity regions below 6.5 m/s. The size of the wakes are normalised against the area of the blade and a ratio between the size of the two regions is also provided to improve comparability and reduce the impact of any measurement inaccuracies. Results for the experiment at 90° and 135° are not provided due to insufficient data available from the original experiment.

It can be seen that at 45° and 270°, there is good agreement between the turbulence models, whilst at 180° *k–ω* SST and transition SST agree with each other but disagree with the similar results of *k–ω* SST LRN and k–k_l–ω that produce a ratio closer to the experimental result. The deviation from the experiment at most positions is poor, although k–k_l–ω and *k–ω* SST LRN demonstrate significantly improved accuracy at 180°, and transition SST at 315°. k–k_l–ω produces

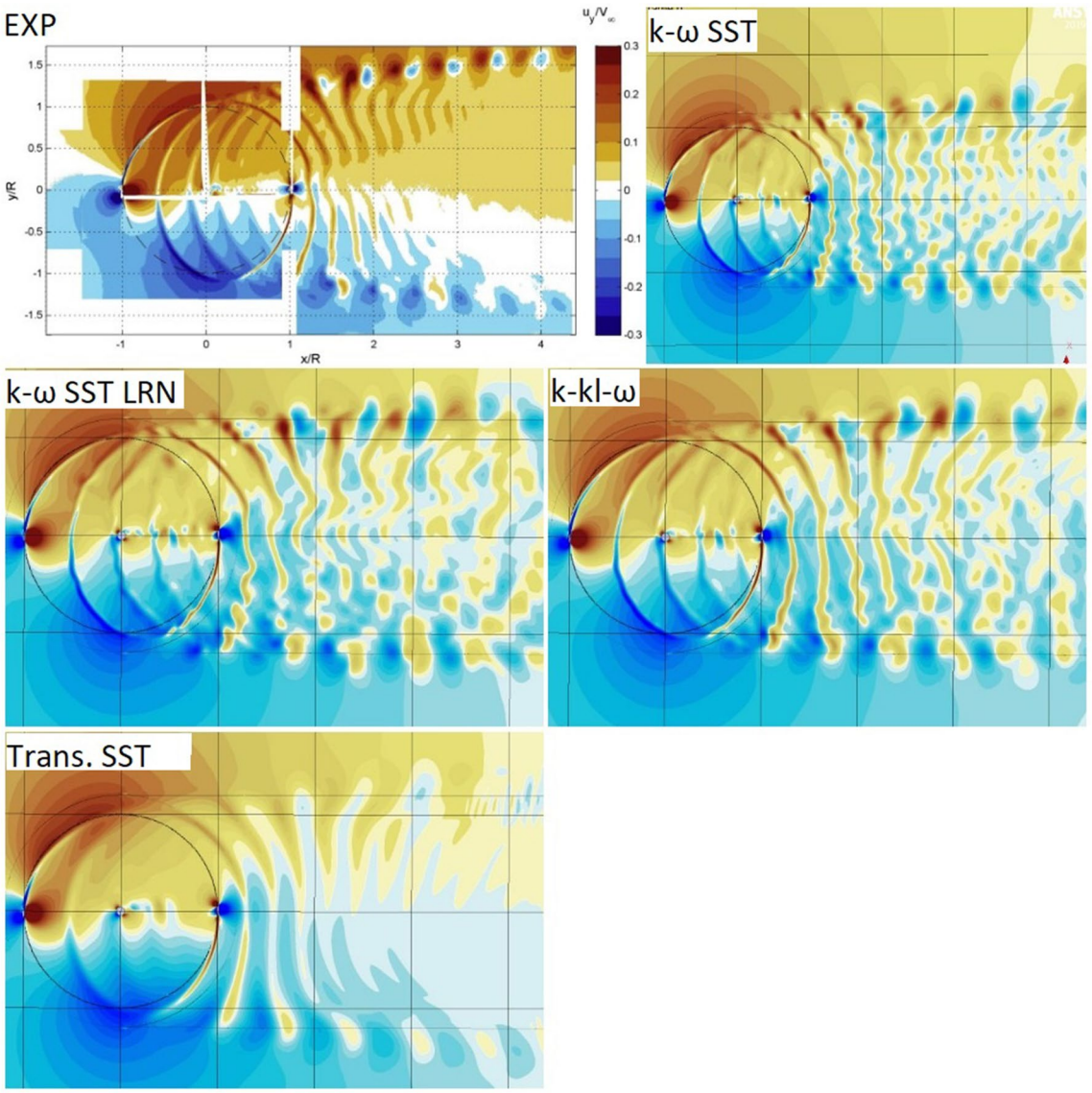

Fig. 14 Comparison of experimental SPIV results for cross-stream velocity by Tescione and CFD results by turbulence model. Upper left: Tescione's results (Tescione et al. 2014), upper right: k–ω SST centre left: k–ω SST LRN, centre right: transition SST, lower: k–k_l–ω

very poor estimates at 0° compared to the other models due to significantly overestimating the size of the high-velocity region.

The average deviations are shown in Table 9, with transition SST offering the lowest deviation. k–k_l–ω has a very high deviation due to the poor estimate at 0°. This deviation at 0° may have contributed to the streamwise velocity underestimate on the downstream wake side in the Tescione validation.

The cause of the quantitative results can then be evaluated qualitatively. In Fig. 16 the experimental velocity values as a ratio of freestream velocity are shown. The original colour scheme used helps to highlight certain flow characteristics but it can also make simulation results look very different if the values are slightly different.

Good agreement is shown between the turbulence models and the experiment at 0° as shown in Fig. 16. At 45° the overall structure of the simulated wakes are similar to the experiment, however, the low-velocity separation is elongated compared to the original teardrop shape in the experiment, as shown in Fig. 17. Results at 90° were not provided for the experiment but good agreement was shown between the turbulence models. Overall, the results for the SST models had insignificant differences between each other, and with all differing significantly from the experiment.

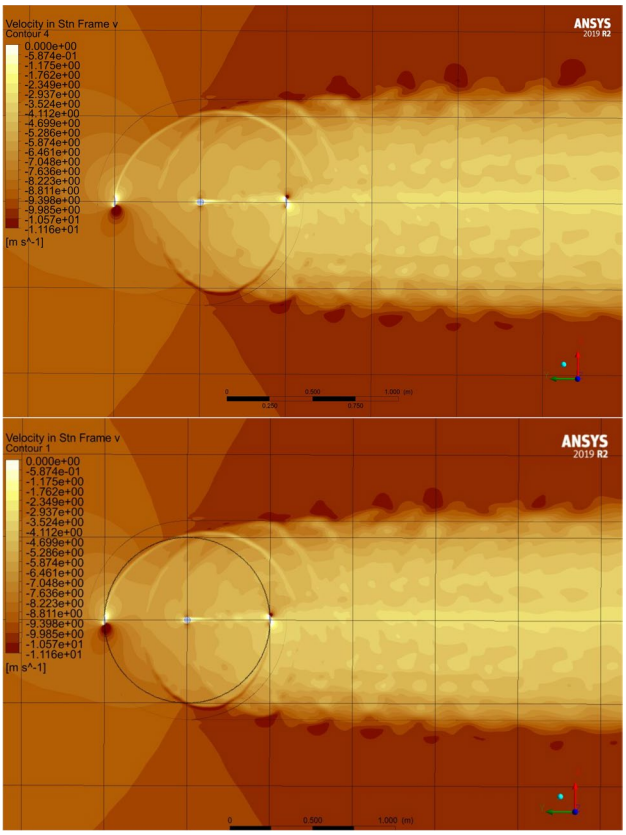

Fig. 15 Comparison between coupled (upper) and SIMPLE (lower) pressure–velocity coupling schemes

At 135°, a small delay in the separation bubble on the inside of the blade is seen in Fig. 18. At 180°, a small high-velocity region is found at the trailing edge which is not present in the experimental results. Using k–k_l–ω, an improvement is seen with a reduction in the size of the high-velocity separation bubble, and increase in the low-velocity separation, at both 135° and 180°, however, they are still different in size to the experimental results as seen in Figs. 18 and 19.

At 225°, a much larger high-velocity region is found at the inner side of the trailing edge of the blade compared to the experiment, seen in Fig. 20. At 270°, the SST turbulence models fail to predict the small separation bubble on the inside of the blade which results in a higher velocity region on the CFD results, as shown in Fig. 21. This issue continues at 315°, shown in Fig. 22.

In all simulations at the 270° position, the direction of the separation bubble at the trailing edge is reversed compared to the experiment, meaning there is a slight difference in the effective angle of attack of the blade. This indicates that there could be a skewed flow in the experiment, which may also have exaggerated other differences between the experiment and CFD results. It is unknown whether this may also be an issue in Tescione's experiment.

At 135° and 225–315°, k–ω SST predicts wider and longer tails than the other models, which is more similar to the experimental results.

Table 8 Comparing the predictions of wake area across a series of azimuthal positions for the tested turbulence models

Condition	Region	Blade area normalised wake area						
Position		0°	45°	135°	180°	225°	270°	315°
Experiment	High region	28.81	7.49	N/A	1.53	0.88	0.82	3.40
	Low region	14.96	4.02	N/A	1.15	0.69	1.87	12.58
	Ratio	1.93	1.87	N/A	1.33	1.27	0.44	0.27
k–ω SST	High region	25.37	7.37	9.98	3.02	0.56	0.61	1.94
	Low region	10.06	3.59	4.83	5.35	2.93	4.90	10.77
	Ratio	2.52	2.05	2.07	0.56	0.19	0.13	0.18
	Deviation (%)	− 30.94	− 10.13	N/A	57.68	85.05	71.53	33.34
k–ω SST LRN	High region	26.79	6.56	11.33	5.24	0.72	0.69	2.05
	Low region	9.44	3.24	4.58	5.38	3.14	5.34	10.65
	Ratio	2.84	2.02	2.48	0.97	0.23	0.13	0.19
	Deviation (%)	− 47.37	− 8.40	N/A	27.12	82.01	70.75	28.75
Transition SST	High region	26.27	7.82	11.75	3.10	0.93	0.63	2.43
	Low region	10.46	3.80	4.44	5.39	3.05	5.52	9.71
	Ratio	2.51	2.06	2.64	0.57	0.30	0.11	0.25
	Deviation (%)	− 30.31	− 10.42	N/A	56.93	75.99	74.05	7.34
k–k_l–ω	High region	35.06	7.59	23.30	4.91	0.95	0.85	1.28
	Low region	9.07	3.65	2.58	5.13	2.61	6.46	9.36
	Ratio	3.86	2.08	9.02	0.96	0.36	0.13	0.14
	Deviation (%)	− 100.56	− 11.54	N/A	28.33	71.43	69.94	49.36

Table 9 Average absolute deviation between simulation and experimental results for Castelein et al.

Turbulence model	Average absolute deviation (%)
k–ω SST	48.11
k–ω SST LRN	44.07
Transition SST	42.51
k–k_l–ω	55.19

3.3.1 Discussion of Castelein validation

Overall, a better prediction of the far-blade wake is seen with transition SST which is expected given that this is similar to the instantaneous results from the Tescione validation, however, there is still significant inaccuracy. It is unclear whether this is due to limitations of the turbulence models, 3D effects, or variables which have not been accounted for.

The difference in results between the turbulence models and the experiment may partially be due to differences in effective angle of attack of the blade, either as a result of the

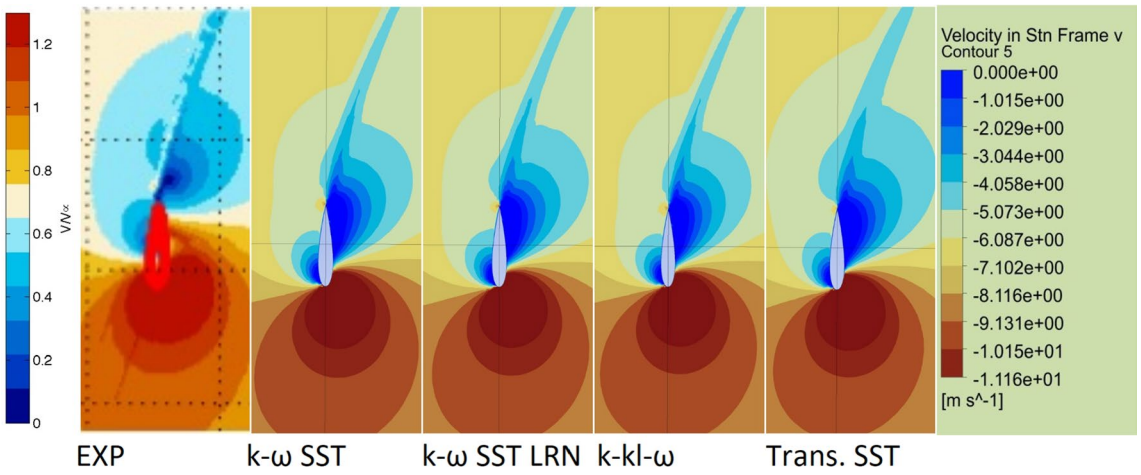

Fig. 16 Velocity at 0° 1: experimental (Castelein et al. 2015), 2: k–ω SST, 3: k–ω SST LRN, 4: transition SST, 5: k–k_l–ω

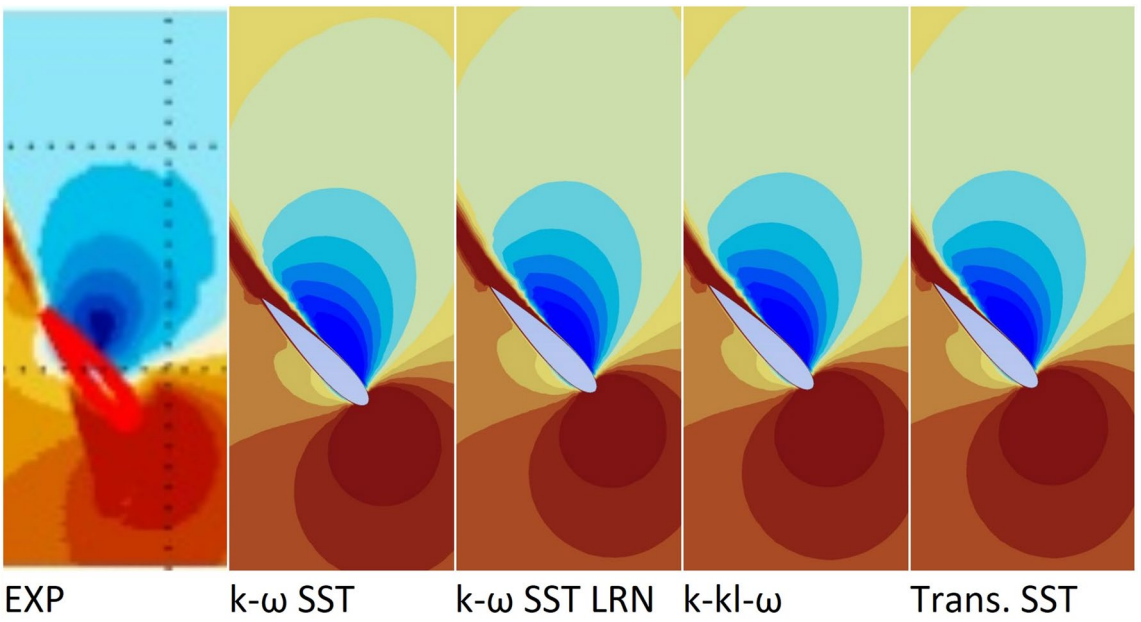

Fig. 17 Velocity at 45° 1: experimental (Castelein et al. 2015), 2: k–ω SST, 3: k–ω SST LRN, 4: transition SST, 5: k–k_l–ω

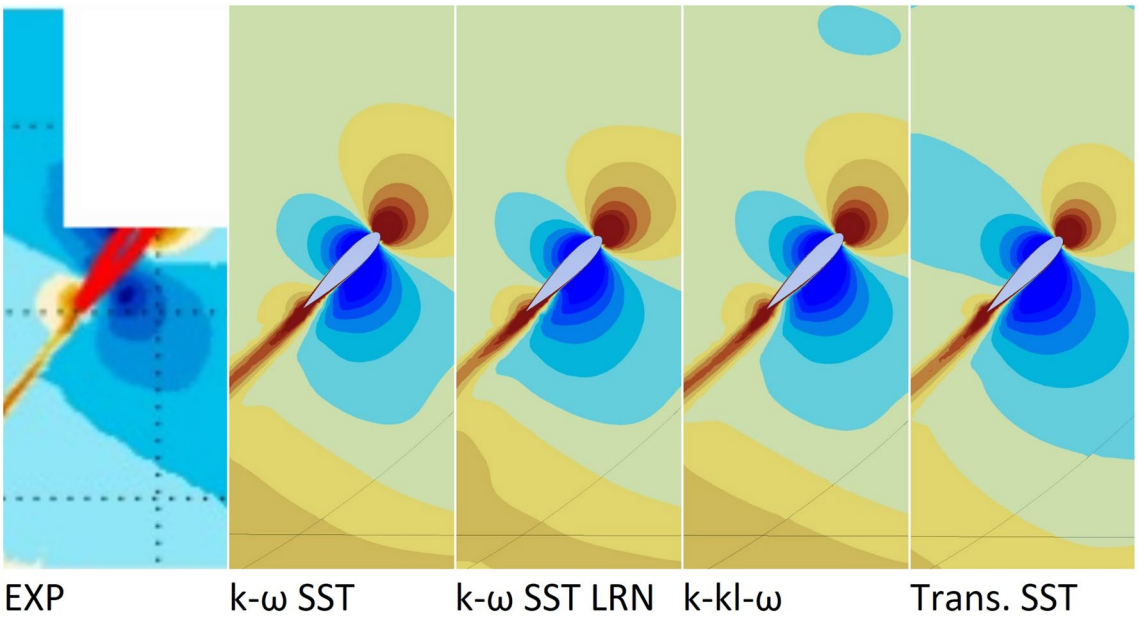

Fig. 18 Velocity at 135° 1: experimental (Castelein et al. 2015), 2: k–ω SST, 3: k–ω SST LRN, 4: transition SST, 5: k–k_l–ω

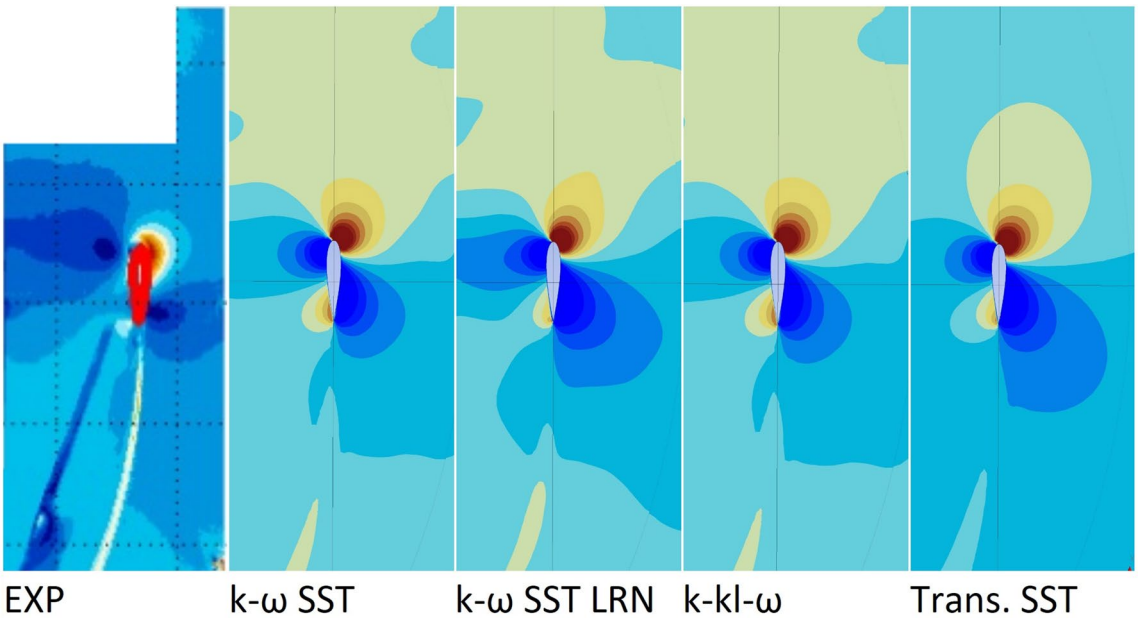

Fig. 19 Velocity at 180° 1: experimental (Castelein et al. 2015), 2: k–ω SST, 3: k–ω SST LRN, 4: transition SST, 5: k–k_l–ω

difference in inlet velocity, the simulation setup, or the wind tunnel setup. Another possible cause is the lack of accounting for surface roughness in the simulations, as Zhang finds that blade wakes are affected significantly by surface roughness (Zhang 2018).

4 Conclusion

From the validations of the three experiments, it has been shown that the 2D modelling techniques used are insufficient for universally accurate prediction of VAWT wakes from near-blade to near-turbine regions. However, this may partially be due to compounding factors in the experiments

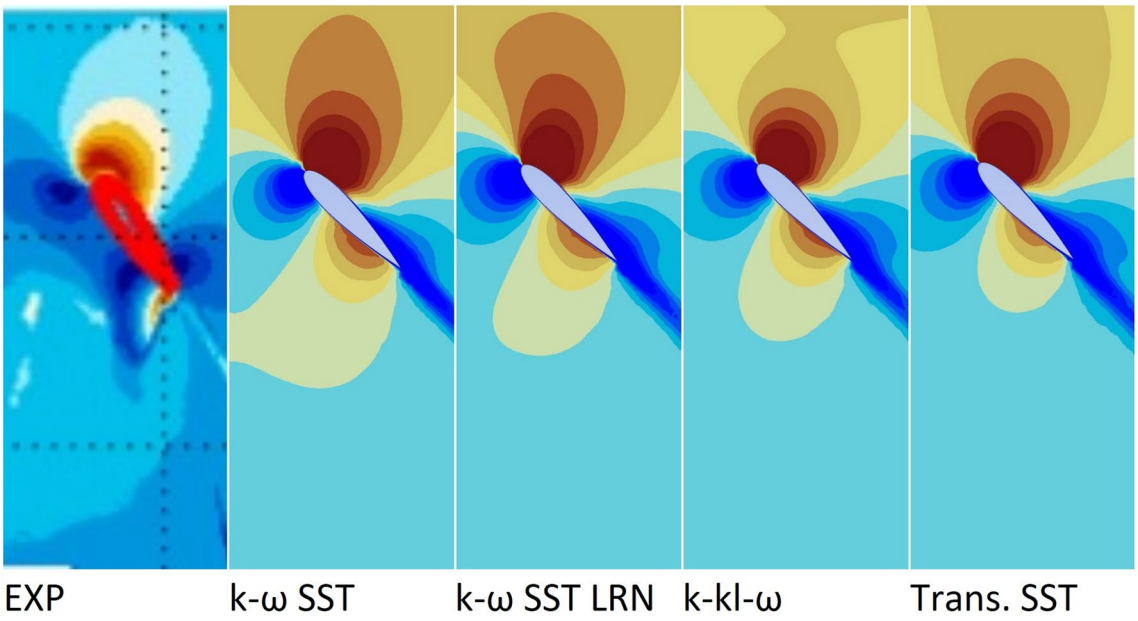

Fig. 20 Velocity at 225° 1: experimental (Castelein et al. 2015), 2: k–ω SST, 3: k–ω SST LRN, 4: transition SST, 5: k–k_l–ω

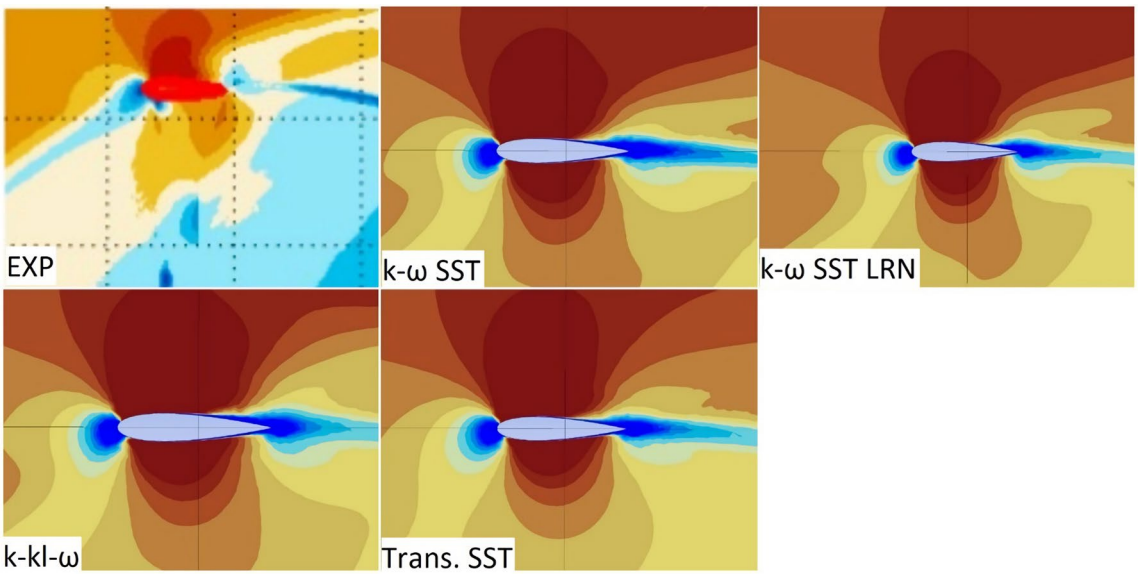

Fig. 21 Velocity at 270° upper: 1: experimental (Castelein et al. 2015), 2: k–ω SST, 3: k–ω SST LRN, lower: 4: transition SST, 5: k–k_l–ω

which have not been accounted for, such as surface roughness and flow in the wind tunnel.

It was possible to identify conditions where 2D CFD produced more accurate results. It was found that the commonly used k–ω SST and k–k_l–ω produce satisfactory results to be used as a faster initial estimate for farm design. Transition SST offers slightly improved accuracy in most circumstances but takes a longer amount of time than k–ω SST. k–k_l–ω can offer improved accuracy in some circumstances including the turbine wake less than 2.5R downstream and for predicting turbulent kinetic energy at low tip speed ratios but it can have poor accuracy in other circumstances as seen at 0° for the high tip speed ratio Castelein validation.

Prediction of VAWT wakes was investigated at scales from the near-blade wake to the near-turbine wake, and across different tip speed ratios to determine the most suitable turbulence model for CFD analysis of VAWTs. CFD

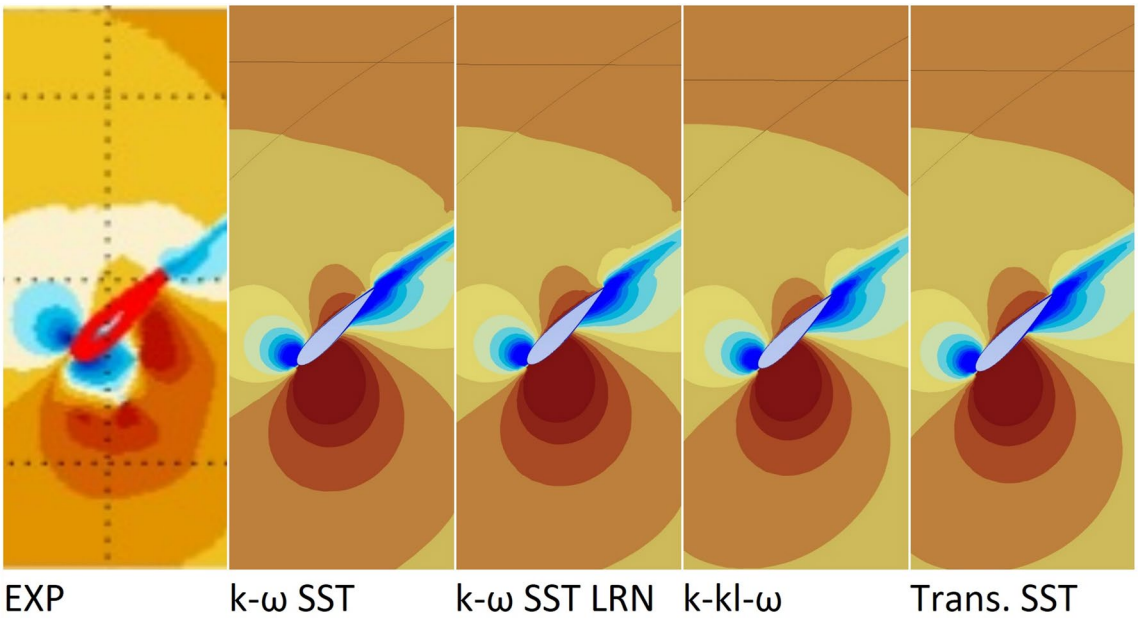

Fig. 22 Velocity at 315° 1: experimental (Castelein et al. 2015), 2: k–ω SST, 3: k–ω SST LRN, 4: transition SST, 5: k–k_l–ω

simulations were conducted based upon three experiments found in the literature which were chosen to represent these conditions.

The necessity of stringent verification procedures for CFD studies of VAWT wakes has also been demonstrated, with very high cell counts being required for good fidelity, and more rigorous definitions necessary for experimental setups if they are to be replicated.

Future research should consider surface roughness and other potentially compounding factors in the experimental setup in VAWT CFD validation, for both 2D and 3D simulations. This may require experimental researchers to be more stringent in defining their setup when they publish their results, such as using a surface roughness comparator to measure surface roughness of the blades used.

- The modelling techniques employed in this study were insufficient for universal accurate prediction of VAWT wakes but scenarios where improved performance is seen have been shown
- Compounding factors are likely to affect results such as insufficient recreation of the baseline experiments in the simulation such as surface roughness and inlet flow
- Future research requires stringent verification procedures and should attempt to measure and account for compounding factors

Acknowledgements This work was supported by an EPSRC Doctoral Training Scholarship.

Funding This research was funded by the EPSRC (Grant no. 2119005).

Availability of data and materials https://doi.org/10.15129/b3038208-436b-4885-8395-0e2b5e1afe47

Declaration

Conflict of interest The authors declare no conflicts of interest.

References

Abdalrahman G, Melek W, Lien F-S (2017) Pitch angle control for a small-scale darrieus vertical axis wind turbine with straight blades (H-Type VAWT). Renew Energy 114(December):1353–1362. https://doi.org/10.1016/J.RENENE.2017.07.068

Almohammadi KM, Ingham DB, Ma L, Pourkashanian M (2013) Effect of transitional turbulence modelling on a straight blade vertical axis wind turbine. In: Ferreira (ed) Alternative energies: updates on progress. Springer, Berlin, pp 93–112. https://doi.org/10.1007/978-3-642-40680-5_5.

Arab A, Javadi M, Anbarsooz M, Moghiman M (2017) A numerical study on the aerodynamic performance and the self-starting characteristics of a Darrieus wind turbine considering its moment of inertia. Renew Energy 107(July):298–311. https://doi.org/10.1016/J.RENENE.2017.02.013

Asr MT, Nezhad EZ, Mustapha F, Wiriadidjaja S (2016) Study on start-up characteristics of H-Darrieus vertical axis wind turbines comprising NACA 4-digit series blade airfoils. Energy 112(October):528–537. https://doi.org/10.1016/J.ENERGY.2016.06.059

Bachant P, Wosnik M (2016) Modeling the near-wake of a vertical-axis cross-flow turbine with 2-D and 3-D RANS. J Renew Sustain Energy 8(5):053311. https://doi.org/10.1063/1.4966161

Balduzzi F, Bianchini A, Maleci R, Ferrara G, Ferrari L (2016) Critical issues in the CFD simulation of Darrieus wind turbines. Renew Energy 85(January):419–435. https://doi.org/10.1016/J.RENENE.2015.06.048

Barnes A, Hughes B (2019) Determining the impact of VAWT farm configurations on power output. Renew Energy. https://doi.org/10.1016/J.RENENE.2019.05.084

Boudreau M, Dumas G (2017) Comparison of the wake recovery of the axial-flow and cross-flow turbine concepts. J Wind Eng Ind Aerodyn 165(June):137–152. https://doi.org/10.1016/j.jweia.2017.03.010

Brownstein ID, Wei NJ, Dabiri JO (2019) Aerodynamically interacting vertical-axis wind turbines: performance enhancement and three-dimensional flow. Energies 12(14):2724. https://doi.org/10.3390/en12142724

Buchner A-J, Lohry MW, Martinelli L, Soria J, Smits AJ (2015) Dynamic Stall in vertical axis wind turbines: comparing experiments and computations. J Wind Eng Ind Aerodyn 146(November):163–171. https://doi.org/10.1016/J.JWEIA.2015.09.001

Castelein D, Daniele R, Giuseppe T, Carlos SF, Ragni D, Tescione G, Simão Ferreira CJ, Gaunaa M (2015) Creating a benchmark of vertical axis wind turbines in dynamic stall for validating numerical models. In: Proceedings of the 33rd Wind Energy Symposium 2015 American Institute of Aeronautics and Astronautics. https://doi.org/10.2514/6.2015-0723

Castelli R, Marco AE, Benini E (2011) The Darrieus wind turbine: proposal for a new performance prediction model based on CFD. Energy 36(8):4919–4934. https://doi.org/10.1016/J.ENERGY.2011.05.036

Dabiri JO (2011) Potential order-of-magnitude enhancement of wind farm power density via counter-rotating vertical-axis wind turbine arrays. J Renew Sustain Energy 3:043104. https://doi.org/10.1063/1.3608170

Danao LA, Qin N, Howell R (2012) A numerical study of blade thickness and camber effects on vertical axis wind turbines. Proc Inst Mech Eng Part A J Power Energy 226(7):867–881. https://doi.org/10.1177/0957650912454403

Danao LA, Edwards J, Eboibi O, Howell R (2014) A Numerical investigation into the influence of unsteady wind on the performance and aerodynamics of a vertical axis wind turbine. Appl Energy 116(March):111–124. https://doi.org/10.1016/J.APENERGY.2013.11.045

Daróczy L, Janiga G, Petrasch K, Webner M, Thévenin D (2015) Comparative analysis of turbulence models for the aerodynamic simulation of H-Darrieus rotors. Energy 90(October):680–690. https://doi.org/10.1016/J.ENERGY.2015.07.102

Ferreira CS (2009) The near wake of the VAWT 2D and 3D views of the VAWT aerodynamics the near wake of the VAWT. TU Delft

Galetta M (2018) Impact of dynamic stall on VAWT performance: implementation into a double multiple stream-tube tool and quantification of model uncertainty. Dissertation, Politecnico di Milano, Milano

Gosselin R (2015) Analysis and optimization of vertical axis turbines. Dissertation, Université Laval

Hand B, Cashman A (2017) Conceptual design of a large-scale floating offshore vertical axis wind turbine. Energy Procedia 142(December):83–88. https://doi.org/10.1016/J.EGYPRO.2017.12.014

Howell R, Qin N, Edwards J, Durrani N (2010) Wind tunnel and numerical study of a small vertical axis wind turbine. Renew Energy 35(2):412–422. https://doi.org/10.1016/J.RENENE.2009.07.025

Iverson D, Boudreau M, Dumas G, Oshkai P (2019) Reprint of: boundary layer tripping on moderate Reynolds number oscillating foils. J Fluids Struct 89:267–278. https://doi.org/10.1016/j.jfluidstructs.2019.102748

Jiang Y, Chenlu H, Peidong Z, Tiezhi S (2020) Investigation of blade tip shape for improving VAWT performance. J Mar Sci Eng. https://doi.org/10.3390/jmse8030225

Kothe LB, Möller SV, Petry AP (2020) Numerical and experimental study of a helical savonius wind turbine and a comparison with a two-stage savonius turbine. Renew Energy 148(April):627–638. https://doi.org/10.1016/j.renene.2019.10.151

Lam HF, Peng HY (2016) Study of wake characteristics of a vertical axis wind turbine by two- and three-dimensional computational fluid dynamics simulations. Renew Energy 90(May):386–398. https://doi.org/10.1016/j.renene.2016.01.011

Lam HF, Peng HY (2017) Measurements of the wake characteristics of co- and counter-rotating twin H-Rotor vertical axis wind turbines. Energy 131(July):13–26. https://doi.org/10.1016/J.ENERGY.2017.05.015

Lee Y-T, Lim H-C (2015) Numerical study of the aerodynamic performance of a 500 W Darrieus-type vertical-axis wind turbine. Renew Energy 83(November):407–415. https://doi.org/10.1016/J.RENENE.2015.04.043

Lei H, Zhou D, Bao Y, Li Ye, Han Z (2017) Three-dimensional improved delayed detached eddy simulation of a two-bladed vertical axis wind turbine. Energy Convers Manag 133(February):235–248. https://doi.org/10.1016/J.ENCONMAN.2016.11.067

Li Q, Takao M, Yasunari K, Junsuke M, Masayuki Y, Tatsuhiko O, Kento S, Tetsuya K (2016) Study on power performance for straight-bladed vertical axis wind turbine by field and wind tunnel test. Renew Energy 90(May):291–300. https://doi.org/10.1016/j.renene.2016.01.002

MacPhee DW, Beyene A (2016) Fluid–structure interaction analysis of a morphing vertical axis wind turbine. J Fluids Struct 60(January):143–159. https://doi.org/10.1016/J.JFLUIDSTRUCTS.2015.10.010

Marten D, Georgios P, Christian NN, Christian OP (2018) Nonlinear lifting line theory applied to vertical axis wind turbines: development of a practical design tool. J Fluids Eng. https://doi.org/10.1115/1.4037978

McLaren K, Tullis S, Ziada S (2012) Computational fluid dynamics simulation of the aerodynamics of a high solidity, small-scale vertical axis wind turbine. Wind Energy 15(3):349–361. https://doi.org/10.1002/we.472

Mohamed OS, Ibrahim AA, Etman AK, Abdelfatah AA, Elbaz AMR (2020) Numerical investigation of Darrieus wind turbine with slotted airfoil blades. Energy Convers Manag X 5(January):100026. https://doi.org/10.1016/j.ecmx.2019.100026

Pan L, Haodong X, Yanwei Z, Zhaoyang S (2020) Research on aerodynamic performance of J-Type blade vertical axis wind turbine. In: 2020 Chinese control and decision conference (CCDC). IEEE, Hefei, China, pp 5454–59. https://doi.org/10.1109/CCDC49329.2020.9164408

Peng HY, Lam HF, Lee CF (2016) Investigation into the wake aerodynamics of a five-straight-bladed vertical axis wind turbine by

wind tunnel tests. J Wind Eng Ind Aerodyn 155(August):23–35. https://doi.org/10.1016/J.JWEIA.2016.05.003

Posa A, Parker CM, Leftwich MC, Balaras E (2016) Wake structure of a single vertical axis wind turbine. Int J Heat Fluid Flow 61(October):75–84. https://doi.org/10.1016/J.IJHEATFLUIDFLOW.2016.02.002

Rezaeiha A, Kalkman I, Blocken B (2017) CFD simulation of a vertical axis wind turbine operating at a moderate tip speed ratio: guidelines for minimum domain size and azimuthal increment. Renew Energy 107(July):373–385. https://doi.org/10.1016/J.RENENE.2017.02.006

Rezaeiha A, Montazeri H, Blocken B (2018) Towards accurate CFD simulations of vertical axis wind turbines at different tip speed ratios and solidities: guidelines for azimuthal increment, domain size and convergence. Energy Convers Manag 156(January):301–316. https://doi.org/10.1016/J.ENCONMAN.2017.11.026

Rezaeiha A, Montazeri H, Blocken B (2019a) CFD analysis of dynamic stall on vertical axis wind turbines using scale-adaptive simulation (SAS): comparison against URANS and hybrid RANS/LES. Energy Convers Manag 196(September):1282–1298. https://doi.org/10.1016/j.enconman.2019.06.081

Rezaeiha A, Montazeri H, Blocken B (2019b) On the accuracy of turbulence models for CFD simulations of vertical axis wind turbines. Energy 180(August):838–857. https://doi.org/10.1016/J.ENERGY.2019.05.053

Rolin V-C, Porté-Agel F (2018) Experimental investigation of vertical-axis wind-turbine wakes in boundary layer flow. Renew Energy 118(April):1–13. https://doi.org/10.1016/J.RENENE.2017.10.105

Sahebzadeh S, Rezaeiha A, Montazeri H (2020) Towards optimal layout design of vertical-axis wind-turbine farms: double rotor arrangements. Energy Convers Manag 226(December):113527. https://doi.org/10.1016/j.enconman.2020.113527

Su J, Yaoran C, Zhaolong H, Dai Z, Yan B, Yongsheng Z (2020) Investigation of V-shaped blade for the performance improvement of vertical axis wind turbines. Appl Energy. https://doi.org/10.1016/j.apenergy.2019.114326

Tescione G, Ragni D, He C, Simão Ferreira CJ, van Bussel GJW (2014) Near wake flow analysis of a vertical axis wind turbine by stereoscopic particle image velocimetry. Renew Energy 70(October):47–61. https://doi.org/10.1016/J.RENENE.2014.02.042

Wahl M (2007) Designing an H-Rotor type wind turbine for operation on amundsen-scott south pole station. Uppsala University

Zanforlin S (2018) Advantages of vertical axis tidal turbines set in close proximity: a comparative CFD investigation in the English channel. Ocean Eng 156(May):358–372. https://doi.org/10.1016/J.OCEANENG.2018.03.035

Zhang Y (2018) Effects of distributed leading-edge roughness on aerodynamic performance of a low-Reynolds-number airfoil: an experimental study. Theor Appl Mech Lett 8(3):201–207. https://doi.org/10.1016/j.taml.2018.03.010